Project No. 12-3361

Coupling of Nuclear Waste Form Corrosion and Radionuclide Transports in Presence of Relevant Repository Sediments

Fuel Cycle

Nathalie A. Wall
Washington State University

In collaboration with:
Pacific Northwest National Laboratory

JC de la Garza, Federal POC
Yifeng Wang, Technical POC

NEUP Nuclear Energy University Programs
U.S. Department of Energy

Final Report

09/30/2015

Coupling of nuclear waste form corrosion and radionuclide transports in presence of relevant repository sediments

Project 12-3361

Principle Investigator: Nathalie A. Wall, Chemistry Department, Washington State University

Co-PI: James J. Neeway, Pacific Northwest National Laboratory; Nikolla P. Qafoku, Pacific Northwest National Laboratory; Joseph V. Ryan, Pacific Northwest National Laboratory

Students who have participated to the project (All WSU):

Undergraduate students: Christopher Musa, Brynden Riggan, Cecilia Eiroa

Graduate students: Lindsey Neill, Joelle Reiser, Jamie Weaver, Nathaniel Murray. Cherilynn Boele

Post-doctoral Fellows: Thomas Lemesle, Benjamin Parruzot

Table of contents

Figure captions

Foreword

The work was originally planned by the Principle Investigator: Nathalie A. Wall (Washington State University) and Co-PIs James J. Neeway (Pacific Northwest National Laboratory), Nikolla P. Qafoku (Pacific Northwest National Laboratory), and Joseph V. Ryan (Pacific Northwest National Laboratory). But we have included two new key members in our scientific conversations and experimental development: Stéphane Gin, Director of Research at the CEA (France) and John McCloy (Associate Professor in the College of Engineering, WSU); these two new team members did not receive any funding from this project.

1 Introduction

Assessments of waste form and disposal options start with the degradation of the waste forms and consequent mobilization of radionuclides. Long-term static tests, single-pass flow-through tests, and the pressurized unsaturated flow test are often employed to study the durability of potential waste forms and to help create models that predict their durability throughout the lifespan of the disposal site. These tests involve the corrosion of the material in the presence of various leachants with different experimental designs yielding desired information about the behavior of the material. *Though these tests have proved instrumental in elucidating various mechanisms responsible for material corrosion, the chemical environment to which the material is subject is often not representative of a potential radioactive waste repository where factors such as pH and leachant composition will be controlled by the near-field environment*. Near-field materials include, but are not limited to, the original engineered barriers, their resulting corrosion products, backfill materials, and the natural host rock. For an accurate performance assessment of a nuclear waste repository, realistic waste corrosion experimental data ought to be modeled to allow for a better understanding of waste form corrosion mechanisms and the effect of immediate geochemical environment on these mechanisms. Additionally, the migration of radionuclides in the resulting chemical environment during and after waste form corrosion must be quantified and mechanisms responsible for migrations understood. The *goal* of this research was to understand the mechanisms responsible for waste form corrosion in the presence of relevant repository sediments to allow for accurate radionuclide migration quantifications. The *rationale* for this work is that a better understanding of waste form corrosion in relevant systems will enable increased reliance on waste form performance in repository environments and potentially decrease the need for expensive engineered barriers.

Our current work aims are 1) quantifying and understanding the processes associated with glass alteration in contact with Fe-bearing materials; 2) quantifying and understanding the processes associated with glass alteration in presence of MgO (example of engineered barrier used in WIPP); 3) identifying glass alteration suppressants and the processes involved to reach glass alteration suppression; 4) quantifying and understanding the processes associated with Saltstone and Cast Stone (SRS and Hanford cementitious waste forms) in various representative groundwaters; 5) investigating positron annihilation as a new tool for the study of glass alteration; and 6) quantifying and understanding the processes associated with glass alteration under gamma irradiation.

2 Multivariable experiments: effect of initial condition of glass and environment on ISG alteration

These experiments are being conducted to determine the influence on the alteration of ISG of a variety of intrinsic and environmental factors in different combinations using a three variable matrix.

The three variables being tested can each take two values, represented in **Table 1** by a + or -, corresponding to the two conditions being tested:

- Leaching solution:
  - Pure water
  - Saturated silica (approx. 150 ppm Si)
- Initial condition of glass:
  - Pristine glass
  - Pre-aged glass (3 month pre-aging)
- Contact between glass and mineral:
  - Direct contact
  - Separated but in contact with same leaching solution.

Three series of experiments are performed, each with one of the three different minerals used: hematite (Fe^{III}), magnetite (Fe^{II} and Fe^{III}), or siderite (Fe^{II}).

Experiment#	Leaching solution	Initial condition of glass	Contact between glass and mineral
1	+	+	+
2	-	-	+
3	+	-	-
4	-	+	-
5	+	+	+
6	-	-	-
7	-	-	-
8	+	-	+
9	-	+	+
10	+	+	-

Table 1: Three variable matrix used for multivariable experiments

2.1 Experimental

Temperature	90°C
Glass form	Powder 100-200 mesh + Coupon in powder bed
S/V ratio	20 cm^{-1} *based on geometric surface area*
Solution composition	18.2 MΩ.cm Water Saturated silica (150 ppm Si)
pH	Free, initial pH = 7
Duration	Static, 9 months

Table 2: Summary of experimental conditions for multivariable studies.

The samples are placed in the oven at 90°C for 9 months with samples taken at 7 time points throughout the duration of the experiment (**Figure 1**). The surface to volume ratio employed is 20 cm^{-1} based on geometric surface area determination. Solution samples are being analyzed by ICP-OES along with pH measurements at each time point.

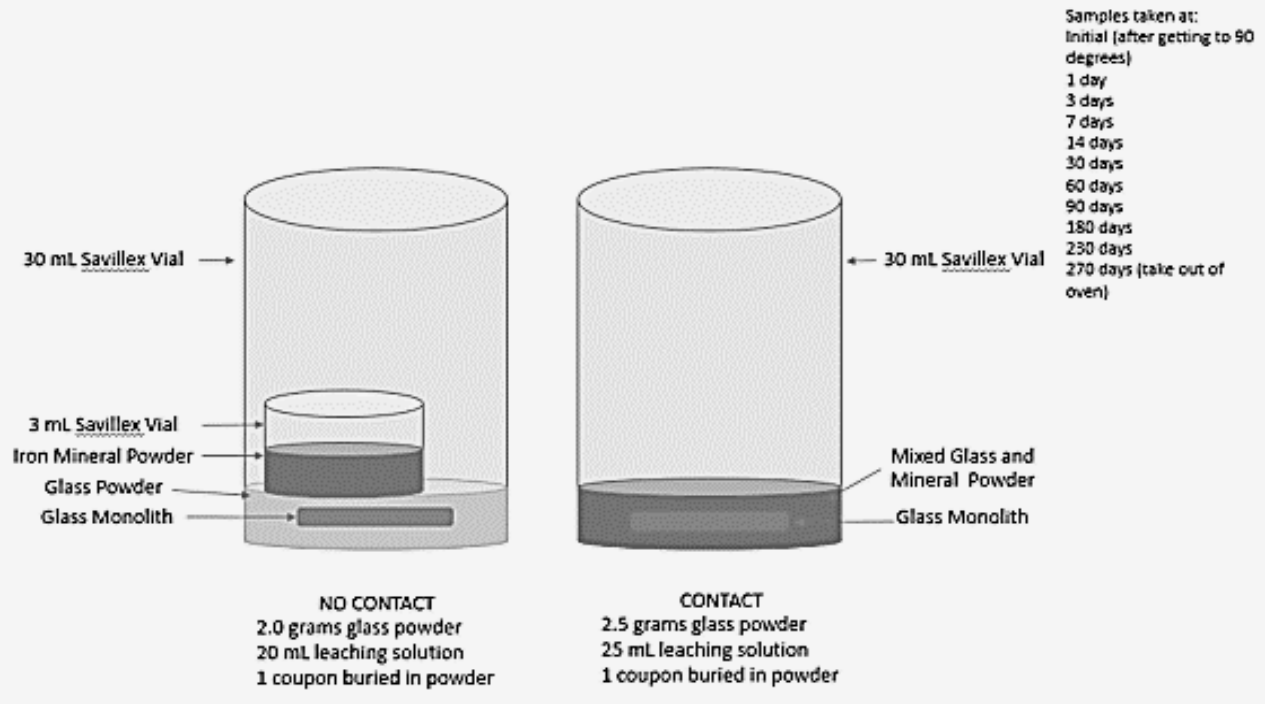

Figure 1: Multivariable setup for alteration of simulated nuclear waste glass with solution

Experiments with hematite and magnetite have already been started, and experiments with siderite are expected to begin in the next month.

2.2 Preliminary results

Preliminary results for ISG alteration with hematite are reported in **Figure 2**. As expected rates are lower for experiments conducted under silica saturated conditions, although the rates begin to stabilize at the same values of those in pure water at about 30 days. There does not seem to be a significant difference between contact and no contact set ups for glass and iron mineral for hematite samples, possibly due to the low solubility of hematite at the near neutral pH of these experiments.

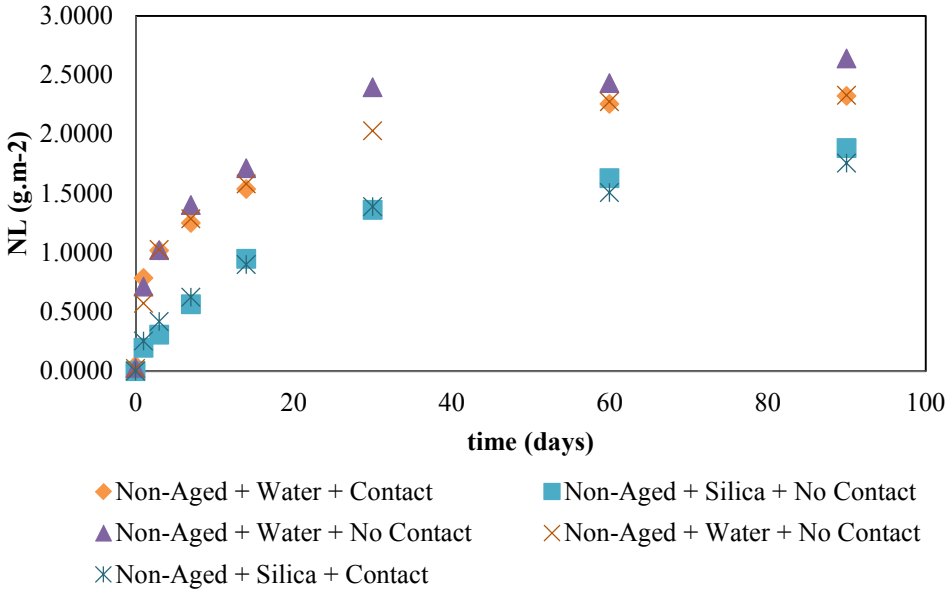

Figure 2: Preliminary solution alteration data for ISG multivariable experiments with hematite

3 Alteration of ISG by a solution containing Fe^{2+} or Fe^{3+}.

These experiments are being conducted to determine the influence of dissolved iron on the alteration of ISG. Preliminary experiments on the corrosion of ISG powders in the presence of an iron salt, $FeCl_3$, solution have been initiated.

Temperature	90°C
Glass form	Powder 100-200 mesh
S/V ratio	20 cm^{-1} *based on geometric surface area*
Solution composition	**** 10^{-4} to 10^{-5} M $FeCl_3$
pH	Free, initial pH = 7
Duration	Static, 9 months

Table 3. Summary of experimental conditions for Iron salt experiments.

Experiments of $FeCl_3$ and ISG are ongoing. Preliminary results have shown that at very high concentrations of $FeCl_3$, very low pH, ISG glass powder dissolve in approximately 30 days. Experiments were performed at lower concentrations of $FeCl_3$ and concentrations of 10^{-4} to 10^{-5} M were found to be ideal. Dissolution of the glasses is much slower at lower concentrations of the salt. Experiments of $FeCl_2$ and ISG are currently being performed under anoxic atmosphere.

4 Glass (ISG or SON68) corrosion in different solutions

Results contained in this section are being written for submission to a peer-review journal.

4.1 Introduction

In this body of work, we focused on glass alterations in five solutions – milliQ water 18.2 MΩ (DIW), NaCl (0.01M and 5M), $CaCl_2$ (0.01M) and $MgCl_2$ (0.01M). These parameters were chosen to quantify and understand glass leaching dissolution as a function of the nature of salt in solution, salt concentration, type of glass, S/V ratio (i.e. surface of glass powder over volume of solution). The goal of this work is to understand leaching dissolution behavior of SON 68 (French glass used for the conditioning of the nuclear HLW) and International Simple Glass (ISG) in salt-bearing solutions.

4.1.1 Experimental procedure

Each set of experiments was duplicated and performed over a 9 months period at 90°C (194°F) in oven. The initial volume of solution in Savillex® vials of 30 mL was 25 mL. The salt-bearing solutions were prepared by dissolving commercial salt in DIW. The glass powders have been obtained by grinding with beads of ZrO_2 or tungsten carbide, sieving over 100-200 meshes (74-149 µm) and cleaned in ultrasonic bath (water then ethanol). The glass monoliths were obtained by cutting and polishing up to 1,200 Grit. pH and ICP-OES measurement of the leaching solution were performed. For the ICP-OES, seven elements were quantified (Si, B, Na, Ca, Fe, Al, Mg and K). 250 µL of leaching dissolution solution were diluted in 1.86 mL of 1.5% of HNO_3 solution. At the end of the 9 months, solid analyses by XRD and SEM will be performed.

The samples were prepared in a horizontal layer pattern, with, from bottom to top of the vial, a glass layer, two glass monoliths, and a mineral layer (**Figure 3**). The ratio between surface of glass (based on BET measurement) and volume of solution was 40 cm^{-1} or 60 cm^{-1}.

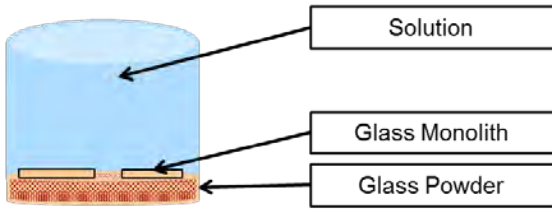

Figure 3: Schematic of the glass alteration experiments

Other samples were prepared in monolith standing vertically. Glasses (powder and monolith: 2.5 g) were altered in solutions of 0.01M of $MgCl_2$, $CaCl_2$, NaCl, or DIW (25 mL). Samples were prepared in a vertical pattern, with the mixed powders at the bottom of the vial and the monoliths were hung by Teflon tape to remain vertical (**Figure 4**). The ratio between surface of glass (based on BET measurement) and volume of solution was 40 cm^{-1} or 60 cm^{-1}.

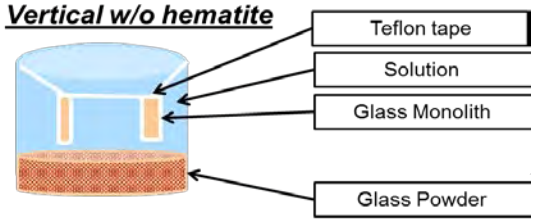

Figure 4. Schematic of the vertical configuration

4.1.2 Results and Discussion

Figure 5 shows pH increase upon addition of glass and slight differences between ISG and SON68 behaviors.

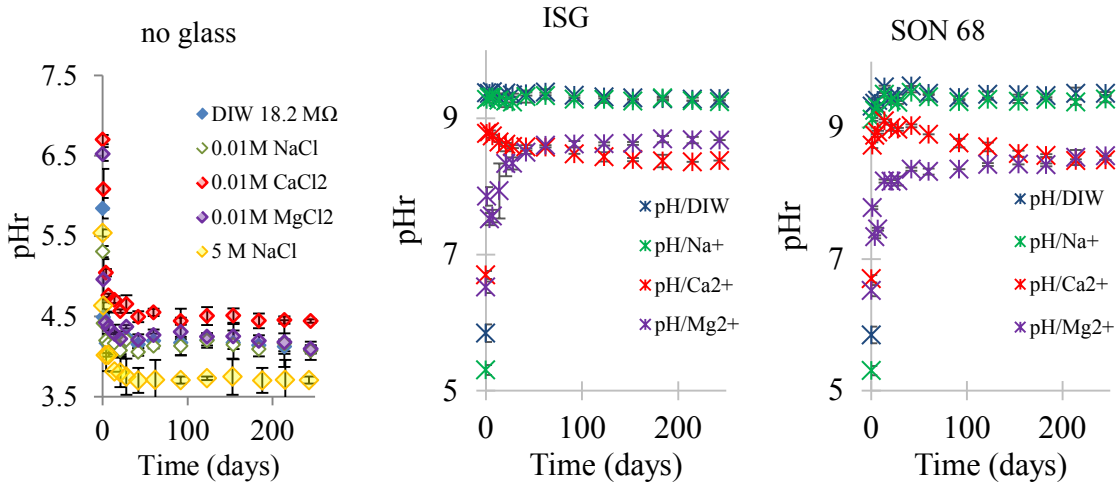

Figure 5. pHr for solutions (in absence of glass); and for ISG or SON68 (60 cm^{-1}) in 0.01 NaCl, $CaCl_2$, $MgCl_2$, and DIW.

Different steps can be distinguished based on the pH evolution plots. The first step is common to all the alteration and corresponds to the increase of the pH during the first day. An increasing pH is due to the glass surface hydration and a desalcalization described by the following equations:

$$\equiv Si - O - Na + H_3O^+ \rightarrow \equiv Si - OH + Na^+ + H_2O \quad (1)$$

$$\equiv Si - O - Na + H_2O \rightarrow \equiv Si - OH + Na^+ + OH^- \quad (2)$$

The second step is due the breaking of the siloxan bonds due to the hydroxyl ion previously created:

$$\equiv Si - O - Si \equiv + H_2O \rightarrow 2 \equiv Si - OH \quad (3)$$

The pH behavior is dependent on the composition of the alteration solution and on the glass composition, especially for the experiments conducted in 0.01 M $MgCl_2$ solution. pH in DIW and 0.01 M NaCl solution are similar. However, glass alteration in NaCl solution lead to less acidic solutions than alteration performed in 0.01 M $CaCl_2$ and 0.01 M $MgCl_2$. We explain this phenomenon by the charge of the electrolyte cation, with the example of Ca^{2+}:

$$2 \equiv Si - OH + Ca^{2+} \rightarrow (\equiv Si - O)_2 = Ca^{2+} + 2H^+ \quad (4)$$

This reaction occurs until there is no Ca^{2+} available or until the pH is around 8.5, corresponding to the pK_a value of the in-plane silanols at 25°C[2]. The aqueous concentration of divalent cations is illustrated on the **Figure 6**; [Ca^{2+}] reaches stability at 400 mg/L (0.01 mol/L) corresponding to the amount initially incorporated in solution – Ca^{2+} is present at 5wt.% in the ISG glass[3] and 4.07wt. %[4] in the SON 68 glass. [Mg^{2+}] decreases during the first 100 days, indicating Mg^{2+} sorption at the surface of the glass.

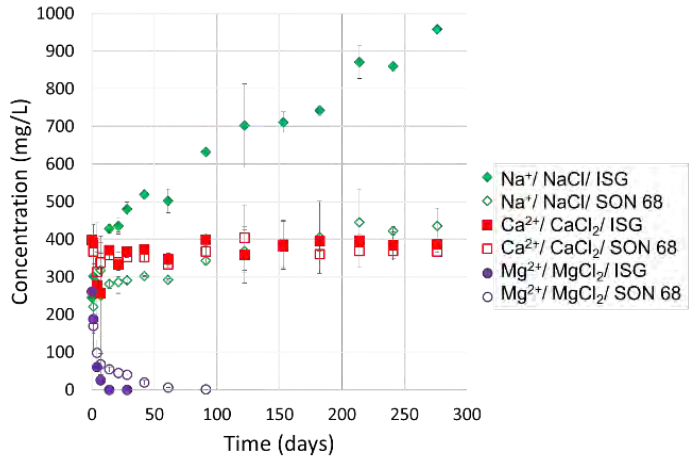

Figure 6. Concentration in Na^+, Ca^{2+} and Mg^{2+} for the alteration in 0.01 M NaCl solution (NaCl), 0.01 M $CaCl_2$ solution ($CaCl_2$), and 0.01 M $MgCl_2$ solution ($MgCl_2$) of the ISG and SON 68 glasses. Surface/Volume = 40 cm^{-1}

For both glasses, a pH increase (**Figure 5**) is observed until the 50th day of experiment, corresponding to the absence of Mg^{2+} in solution (**Figure 6**). No difference was observed on the pH evolution between alteration of ISG glass and SON 68 glass except for experiments performed in 0.01 M $MgCl_2$ solution (**Figure 5**) – pH is lower for SON 68 samples. The pH difference between ISG and SON 68 can be explained by sorption of +III cations: [5]

$$2 \equiv Si - OH + M^{3+} \rightarrow 2SiO_2{-}M^{+} + 2H^{+} \qquad (5)$$

Trivalent elements sorption release H^+ in solution, but the minimal amount of +III cations (except B^{3+} and Al^{3+}) in the composition of the ISG glass[3] leads to higher pH than for SON68 experiments.

Figure 8 presents the equivalent thickness (based on the boron released in solution, measured by ICP-OES) as a function of time, for the alteration of the ISG and SON 68 in DIW, 0.01 M NaCl, 0.01 M $CaCl_2$ and 0.01 M $MgCl_2$. The equivalent thickness (ET_i) corresponds to the thickness of the layer of altered glass and is calculated with the equation below:

$$ET_i = \frac{NL_i}{\rho} \qquad (9)$$

NL_i corresponds to the normalized mass loss based on the "i" element release and ρ corresponds to the density of the glass. ISG Normalized mass losses are presented on **Figure 7**. $MgCl_2$ induces the largest normalized mass loss and $CaCl_2$ the smallest.

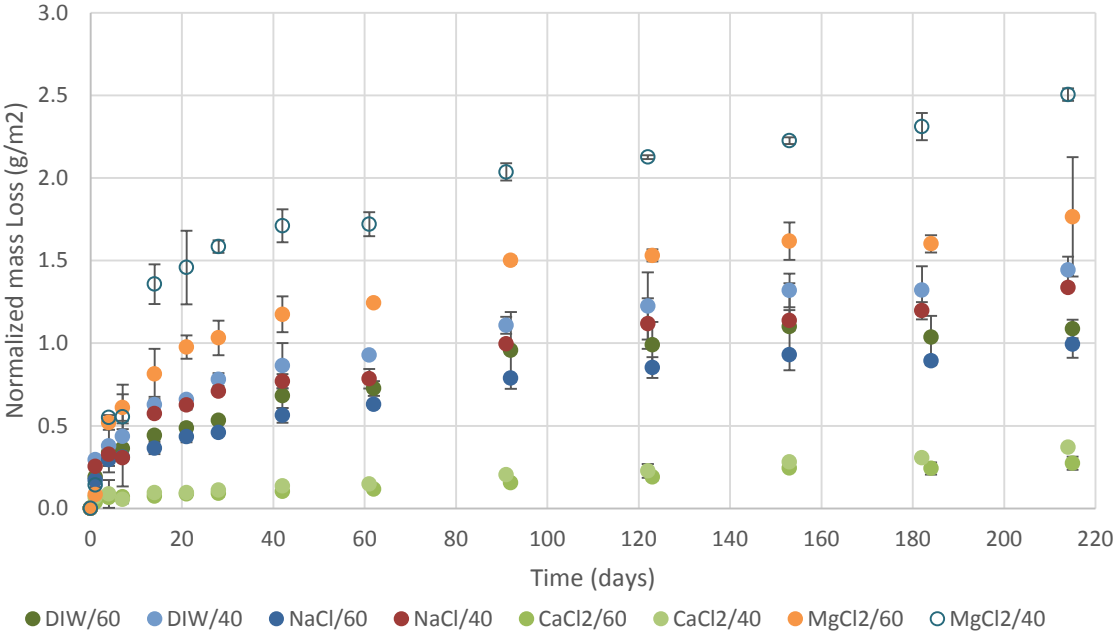

Figure 7. ISG Normalized mass Loss as a function of time, for 40 and 60 cm^{-1} S/V ratios and different solutions

Alterations in $MgCl_2$ solution lead to larger thickness than in $CaCl_2$ solution. The literature showed similar results, with the explanation that aqueous Ca^{2+} cations react with the Si present in the hydrated surface layer forming a passivating reactive interphase,[6] a phenomenon which does not occur in $MgCl_2$ solution due to pH remaining below 9 (**Figure 5**). The largest equivalent thickness is found for 0.01 M $MgCl_2$ solutions (specifically larger than in DIW), while Si released in solution (**Figure 9**) is very similar between experiments in 0.01 M $CaCl_2$ and 0.01 M $MgCl_2$. To explain the effect of the presence of $MgCl_2$ in solution, Majerus et al. proposed that contrary to Ca^{2+} cations, Mg^{2+} cations lead to a destabilization of the hydrated surface layer that hiders its global densification and decreases its passivating role.[7] This phenomenon has been demonstrated by the observation of a more porous layer for the experiments performed in $MgCl_2$ solution.

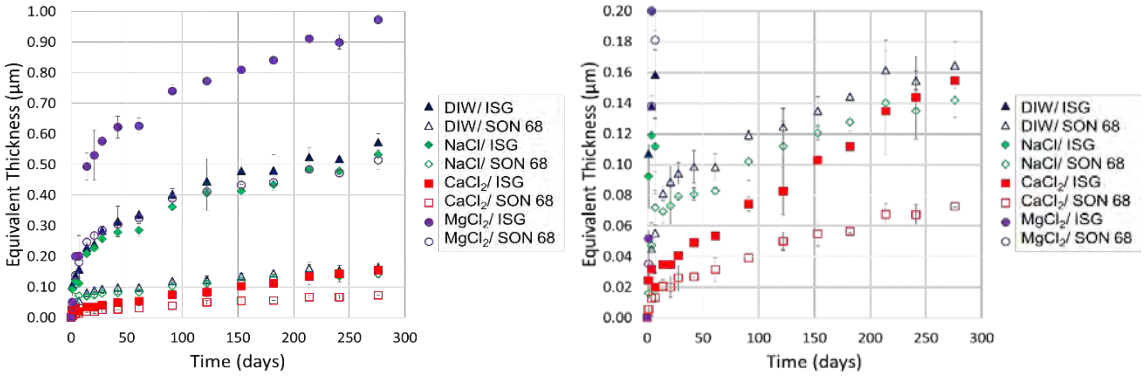

Figure 8. Equivalent thickness based on boron released in solution as a function of time for the alteration in DIW, 0.01 M NaCl solution (NaCl), 0.01 M $CaCl_2$ solution ($CaCl_2$) and 0.01 M $MgCl_2$ solution ($MgCl_2$) of the ISG and SON 68 glasses. The graph on the right represents an enhancement of the graph on the left; Surface / Volume = 40 cm^{-1}.

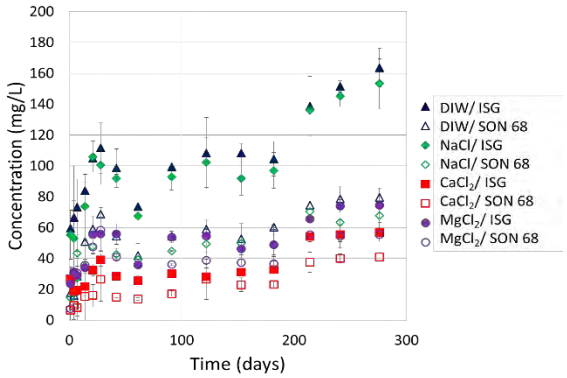

Figure 9. Concentration in Si^{4+} as a function of time for the alteration in 0.01 M NaCl solution (NaCl), 0.01 M $CaCl_2$ solution ($CaCl_2$), and 0.01 M $MgCl_2$ solution ($MgCl_2$) of the ISG and SON 68 glasses; Surface / Volume = 40 cm^{-1}

The alteration layer is ca. 0.5 µm after 9 months of SON 68 alteration, a value confirmed by SEM analyses (**Figure 10**). SEM picture shows two alteration layers: "Alteration Layer 1" is porous, probably due to the presence of Mg^{2+} "Alteration Layer 2" represents a more hydrated layer close to the pristine glass.

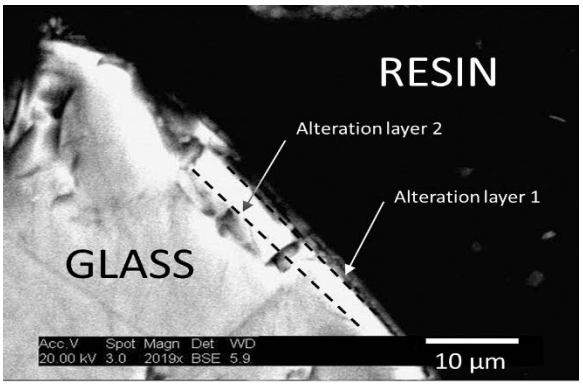

Figure 10. SEM picture performed in BSE of a grain of SON 68 glass powder altered 9 months in 0.01 M $MgCl_2$ solution; Surface / Volume = 40 cm^{-1}

The leaching dissolution rate was calculated, specifically the rate between the 3th month and the 9th month of experiments. This rate has been qualified be the residual rate due to its stability over this time period. **Figure 11** shows similar rates between glass alteration in DIW and in 0.01 M NaCl solution at ca. $3 \cdot 10^{-3}$ $g \cdot m^{-2} \cdot d^{-1}$. As for the boron equivalent thickness, alteration rates in $CaCl_2$ are much lower than in DIW and much higher in $MgCl_2$ than in DIW. Although the

dissolution be mainly driven by the hydrolysis of the silica-oxygen bonds, the reaction with the alkaline earth cations has an important role. According to the pH plot, the phenomenon which occurred at the surface of the glass could change and modify the behavior of the glass in term of dissolution rate. For a $pH_{90°C}$ at 9, incorporation of cation in the gel passivating layer is probable, as expected in the case of Ca^{2+}.[6] Below pH 9, the phenomenon which occurs in the reaction is the formation of Mg-Si phases as described by Thien and al..[8] The formation of Mg-Si phases consumes the silica released by the glass and Si does not remain in the gel layer. It explains why the passivating properties decrease and involve a decrease of the dissolution rate in 0.01 M $MgCl_2$ solution. The alteration rate in 0.01 M NaCl solution is similar to the alteration in DIW because the dissolution is mainly driven by the exchange between the Na^+ from the glass and the solution. Similar studies with an S/V ratio of 60 cm^{-1} were performed and confirmed the results presented for 40 cm^{-1}.

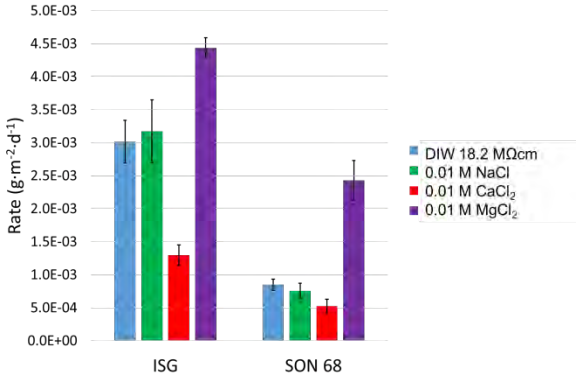

Figure 11. Leaching dissolution rate for the residual rate based on the boron released for the alteration in deionized water (DIW 18.2 MΩ cm), 0.01 M NaCl solution (NaCl), 0.01 M $CaCl_2$ solution ($CaCl_2$) and 0.01 M $MgCl_2$ solution ($MgCl_2$) of the ISG and SON 68 glasses; Surface / Volume = 40 cm^{-1}

According to **Figure 8**, the boron equivalent thickness (ET_B) is larger for the alteration of ISG than for that of SON 68. The ratio between the equivalent thickness of SON 68 alteration and ISG alteration is ca. 3.73 after the 9 month experiments (ET_B(ISG)/ET_B(SON 68)) in DIW and 0.01 M NaCl (3.720 and 3.753 respectively) and lower for the alteration in $CaCl_2$ and $MgCl_2$ solutions (1.889 in 0.01 M $MgCl_2$ and 2.109 in 0.01 M $CaCl_2$). Gin and al. also showed higher equivalent thicknesses for the ISG glass (called CJ4 in their publication) than for SON 68 (ratio of ca. 4) in DIW.[9]

The spherical shrinking-core model was used to calculate the leaching dissolution rate; it accounts for the reduction of the surface of the grain over time. The rate (R_i) and the normalized mass loss (NL_i) from the concentration of the element "i" measured by ICP-OES in solution were obtained via the following equations:

$$NL_i = \frac{3\times(1-(1-\%alt_i)^{1/3})}{S_{BET}} \quad (6)$$

Where S_{BET} is the BET surface of the glass powder (m^2/g) and $\%alt_i$ is the altered fraction of glass based on the "i" element given by:

$$\%alt_i(t_\alpha) = \frac{C_i(t_\alpha)\times V(t_\alpha)}{m_{glass}\times \%m_i} + \%alt_i(t_{\alpha-1}) \quad (7)$$

Where $C_i(t_\alpha)$ the concentration (g/m^3) of i element at the t_α time, $V(t_\alpha)$ the volume (m^3) of solution at the t_α time, m_{glass} the initial glass powder mass and, $\%m_i$ the mass percentage of element i present within the glass composition.

The leaching dissolution rate based on the element i ($g/m^2/d$) is the derivative of the normalized mass loss (NL_i) as a function of time:

$$R_i = \frac{dNL_i}{dt} \quad (8)$$

The initiation of the residual rate is determined as explained by Gin et al.[9], where the dissolution rate is plotted as a function of boron released and as a function of the H_4SiO_4 concentration. The residual rate initiates when a deviation from the first order rate law is observed. **Figure 12** shows two examples plots to illustrate variations for start of residual rates with the system studied. The residual rate may initiate at different day (**Table 4**), we chose to adopt the latest residual rate start day to calculate systematically the residual rate between the 3rd and the 9th month of experiment, based on boron concentration – boron is considered as a 'tracer' for the dissolution because of its release in solution and lack of retention in secondary phases or in gel layer. The leaching dissolution rate is calculated as the average of all the rates estimated between each month sampling time (average of 7 data). Data associated errors correspond to 2σ (95% statistical confidents).

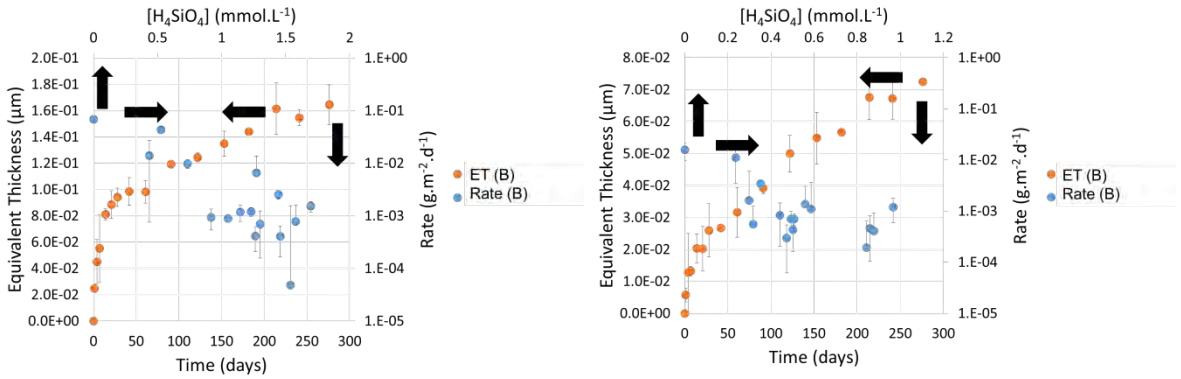

Figure 12. Equivalent thickness based on boron released (ET (B)) as a function of time and associated leaching dissolution rate (based on released boron) as a function of H_4SiO_4 concentration (Rate (B)) for the alteration experiments of SON 68 glasses in DIW (left) and 0.01 M $CaCl_2$ solution (right) (Surface/Volume ratio (S/V) 40 cm^{-1})

Name	Day of stabilization	Rate ($g.m^{-2}.d^{-1}$)	$[H_4SiO_4]$ ($mmol.L^{-1}$)
DIW-ISG	60^{th}	$5 \cdot 10^{-3}$	1.64
0.01 M NaCl-ISG	60^{th}	$5 \cdot 10^{-3}$	1.50
0.01 M $CaCl_2$-ISG	28^{th}	$1 \cdot 10^{-3}$	0.69
0.01 M $MgCl_2$-ISG	92^{nd}	$5 \cdot 10^{-3}$	1.34
DIW-SON 68	92^{nd}	$1 \cdot 10^{-3}$	1.10
0.01 M NaCl-SON 68	42^{nd}	$1 \cdot 10^{-3}$	1.00
0.01 M $CaCl_2$-SON 68	28^{th}	$7 \cdot 10^{-4}$	0.49
0.01 M $MgCl_2$-SON 68	92^{nd}	$4 \cdot 10^{-3}$	1.35

Table 4. Estimated start of the residual rates (day of stabilization) and associated leaching dissolution rate (Rate) and concentration in H_4SiO_4 ($[H_4SiO_4]$) for the 8 experiments performed with an S/V ratio of 40 cm^{-1}.

5 Glass (ISG or SON68) corrosion in contact with hematite and siderite

Results contained in this section are being written for submission to a peer-review journal.

5.1 Introduction

In this body of work, we focused on glass alterations in five solutions – DIW, NaCl (0.01M and 5M), $CaCl_2$ (0.01M) and $MgCl_2$ (0.01M) – and in presence of two types of Fe-bearing minerals – hematite and siderite. The studies on siderite have been performed under inert atmosphere to avoid Fe(II) oxidation; hematite experiments were performed under atmospheric level of oxygen.

Glass leaching dissolution were tested as a function of the nature of salt in solution, salt concentration, type of glass, S/V ratio (i.e. surface of glass powder over volume of solution) and presence of mineral.

5.1.1 Experimental procedure

Experimental set-ups were similar to that in absence of minerals, described in the section above.

Schematics are presented below. SON 68 and ISG were studied. Each set of experiments was duplicated and performed over a 9 months period at 90°C (194°F) in oven. The initial volume of solution in Savillex® vials of 30 mL was 25 mL. The salt-bearing solutions were prepared by dissolving commercial salt in DIW. The glass powders have been obtained by grinding with beads of ZrO_2 or tungsten carbide, sieving over 100-200 meshes (74-149 µm) and cleaned in ultrasonic bath (water then ethanol). The glass monoliths were obtained by cutting and polishing up to 1,200 Grit. The hematite and the siderite were obtained commercially and crushed in mortar before sieving over 270-325 meshes (45-53 µm) using a mechanical shaker. pH and ICP-OES measurement of the leaching solution were performed. For the ICP-OES, seven elements were quantified (Si, B, Na, Ca, Fe, Al, Mg and K). 250 µL of leaching dissolution solution were diluted in 1.86 mL of 1.5% of HNO_3 solution. At the end of the 9 months, solid analyses by XRD and SEM will be performed.

Two sets of hematite experiments were performed: with 0.1 g and with 1 g. The hematite incorporated in the Savillex® vials is hematite powder with a specific surface of 0.019 m^2/g. The alterations tests was performed in DIW, NaCl (0.01M), $CaCl_2$ (0.01M), and $MgCl_2$ (0.01M).

The samples were prepared as seen in **Figure 13**. The ratio between surface of glass (based on BET measurement) and volume of solution was 40 cm^{-1} or 60 cm^{-1}. Experiments were also prepared with mineral in solution, without glass.

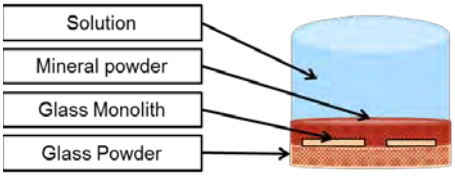

Figure 13: Schematic of the Glass alteration in presence of mineral

5.1.2 Results and discussion

Figure 14 illustrates the evolution of the pHr over time in solutions containing 0.01 M salt or water and various amounts of hematite. The presence of hematite in solution promotes an increased pHr, correlated to the hematite concentration. In presence of 1 g of hematite pHr is at its highest and the trend is $MgCl_2 < CaCl_2 < NaCl < DIW$.

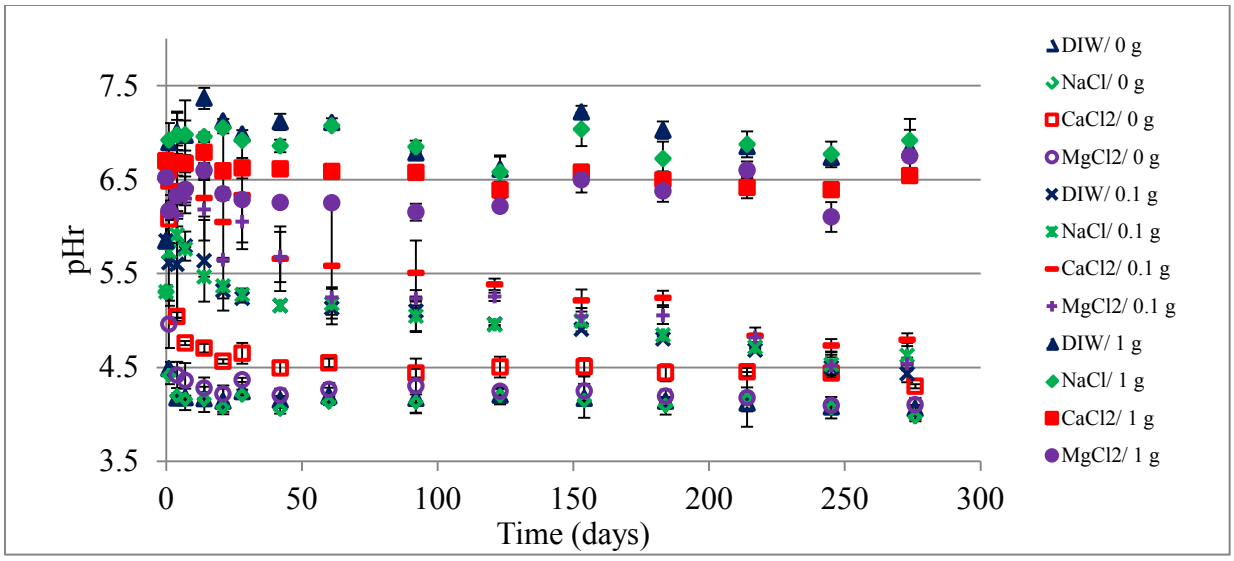

Figure 14. pH_r in 0.01 M salt solution or water over time as a function of the amount of hematite present [label Na+/ 0 g indicates: alteration of 0 g of hematite in a 0.01 M NaCl solution]

Figure 15 presents pHr values for ISG and SON68 alteration in DIW or 0.01 M $CaCl_2$ or $MgCl_2$ at 40 or 60 cm^{-1}. SON68 lead to higher solution pH than ISG; solution pH values are not affected by the presence of glass, except for SNO68 in $MgCl_2$, for which the presence of 0.1 g hematite decreases the solution pH; a change of S/V from 40 to 60 cm^{-1} has negligible effect on solution pH values; pH of Ca and Mg solution systematically equilibrate at a value below 9 while pH > 9 for DIW and NaCl; Mg solutions equilibrate at higher pH than Ca solutions for ISG, but both solutions equilibrate at similar pH for SON68.

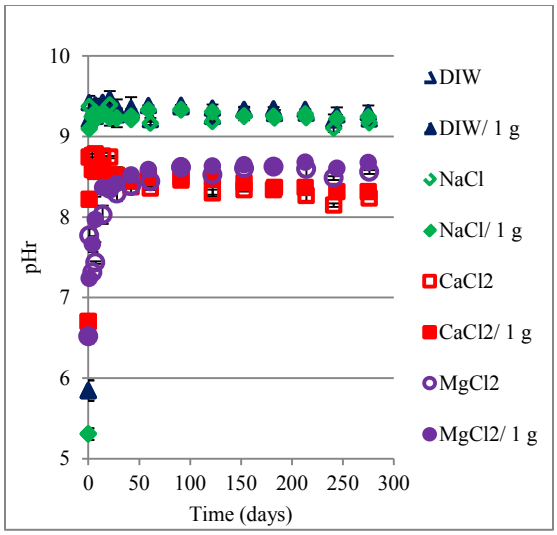

A. ISG-S/V=40 cm-1, in 0.01 M salt solution or water

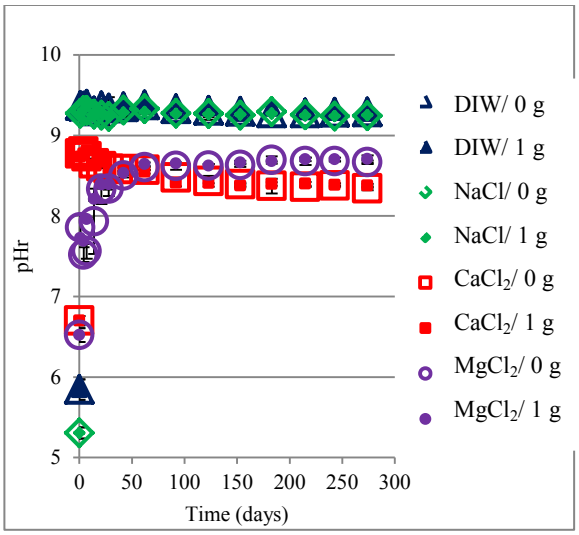

B. ISG-S/V=60 cm-1, in 0.01 M salt solution or water

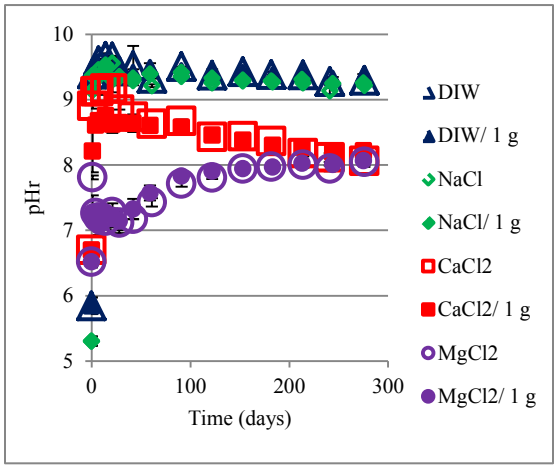

C. SON68-S/V=40 cm-1, in 0.01 M salt solution or water

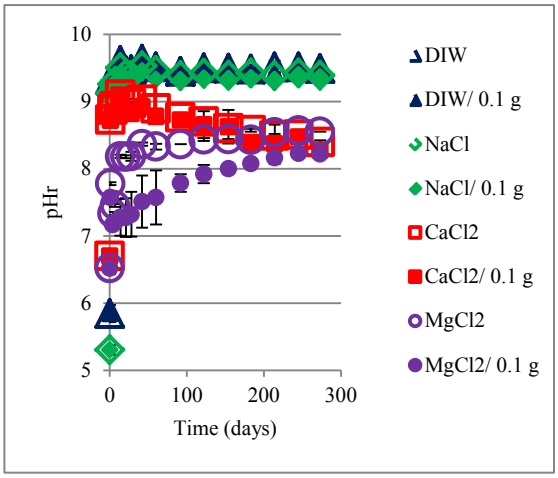

D. SON68-S/V=60 cm-1, in 0.01 M salt solution or water

Figure 15. pHr for ISG and SON68 alteration in DIW or 0.01 M $CaCl_2$ or $MgCl_2$ at 40 or 60 cm^{-1}, in presence or absence of hematite.

Leaching dissolution rates were calculated with equation (3) and presented in **Figure 16**. Hematite appears to decrease dissolution rates on average in all solutions, although the errors are sometime too large to confirm. ISG Normalized mass Losses as a function of time in presence of 0.1 g hematite is presented in **Figure 17** are virtually identical to those in absence of hematite, shown on **Figure 7**.

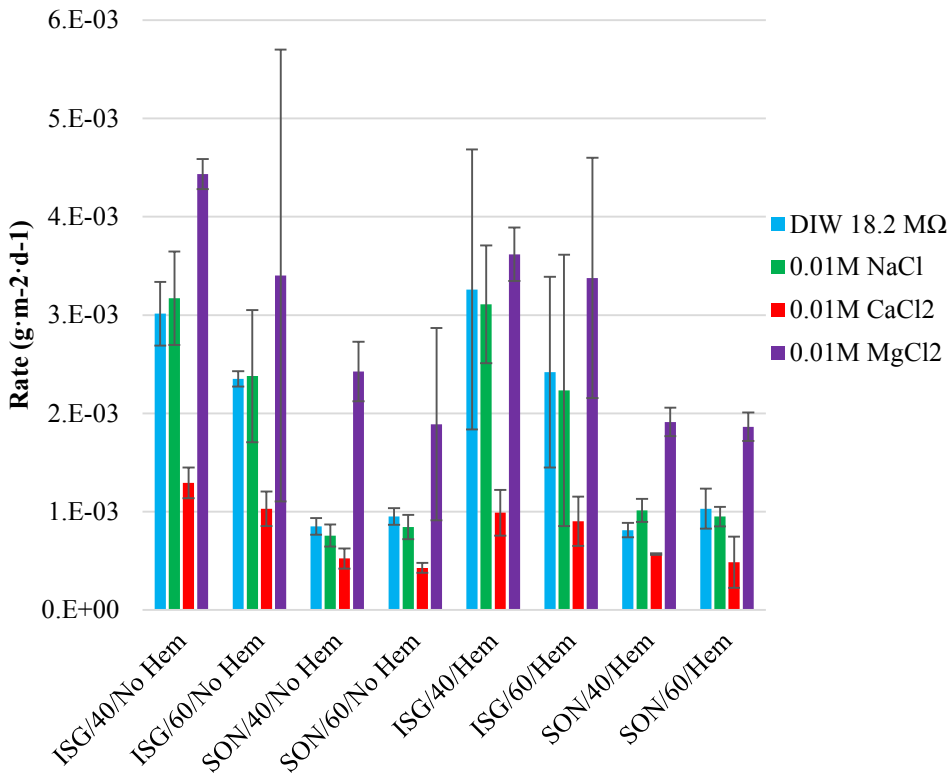

Figure 16. Leaching dissolution rate for the residual rate based on the boron released for the alteration in DIW, 0.01 M NaCl solution (NaCl), 0.01 M $CaCl_2$ solution ($CaCl_2$) and 0.01 M $MgCl_2$ solution ($MgCl_2$) of the ISG and SON 68 glasses, in presence and absence of hematite

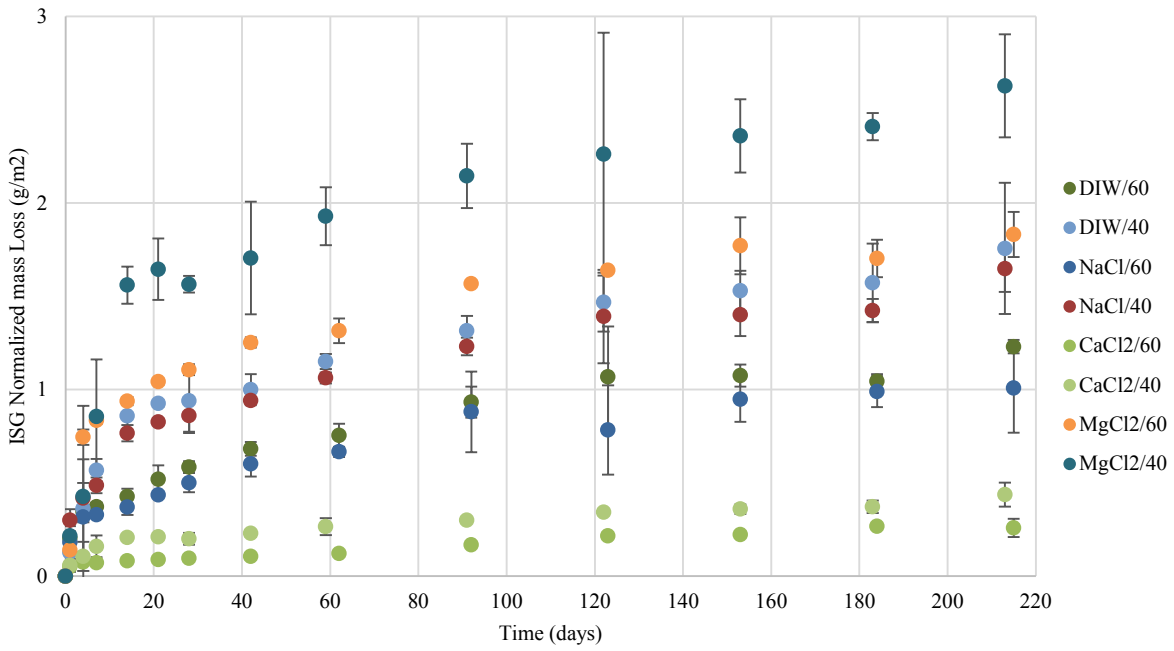

Figure 17. ISG normalized mass Loss as a function of time in presence of 0.1 g hematite, and for 40 or 60 cm^{-1} S/V ratios.

The absence of a measurable effect of hematite on the leaching dissolution rate can be explained by the fact that there was no alteration of the hematite during the first 42 days – we observe negligible amount of iron released in solution during its alteration for 42 days.

Experiments in presence of siderite and under inert atmosphere have been initiated, but not yet completed.

6 Glass alteration in presence of MgO

MgO is used as an engineered barrier in the Waste Isolation Pilot Plant to buffer pH and convert $CO_{2(g)}$ into a solid phase ($MgCO_3$). The effect of three separate iron sources on the corrosion of ISG and SON68 submerged in saturated and pH adjusted MgO solution is currently under study. The three iron sources are hematite (Fe^{3+}), for which preliminary experiments have already been executed, iron powder of ~ 70 mesh (Fe^0), and iron chloride salt (Fe^{3+}). These three forms of iron were chosen because they have been hypothesized to be present near-field to stored nuclear waste glass.[10] The source of the iron in the aforementioned repository settings could be derived from the stainless steel canisters used to hold the glass. The reactivity of ISG with iron in the presence of MgO is of interest due to use of magnesium oxide overpacks at the Waste Isolation Pilot Plant (WIPP) in Carlsbad, NM.

6.1 Method

Temperature	90°C
Glass form	Powder 100-200 mesh + Coupon in powder bed
S/V ratio	20 cm^{-1} *based on geometric surface area*
Solution composition	Saturated MgO
pH	****
Duration	Static, 9 months

Table 5. Summary of experimental conditions for alteration of ISG in saturated MgO solution

ISG glass lingot was cut into coupons with an oil (IsoCut™ Fluid, Buehler) lubricated diamond saw (IsoMet™ Low Speed Saw, Buehler). Approximate dimensions of the coupons were 30 mm × 10 mm × 4 mm. Each coupon was polished at 120, 320, 600, and 1200 grits using an oil-based lubricant (IsoCut™ Fluid, Buehler) on a Leco™ Grinding and Polishing Polisher. Glass powders were made by crushing ISG in a tungsten carbide mill (Angstrom) for 2 seconds. The glass powders were then sieved to 100-200 mesh particle sizes, and ultrasonically washed three times in dry ethanol. The wet powders were then dried to a constant weight in a 90˚C oven. $FeCl_3$ and the Iron powder were purchased from Fisher Scientific. The iron powder was also ultrasonically washed in dry ethanol three times, and dried to a constant weight at 90˚C to remove any fines. The iron salt was used as received.

Each experiment was setup using the multivariable matrix protocol (**Figure 1**). The experiments were defined as either “in contact” or with “no contact”. Each experiment set used approximately 2.0 grams of powder to 20.0 mL of solution or 2.5 grams of powder to 25.0 mL of solution. A monolith of glass was introduced inside the glass powder bed in each experiment. These experiments are to run for 270 days at 90˚C. Sample blanks were executed alongside the experiments.

Sampling has been conducted as listed in **Figure 1.** pH measurements and 250 μL of solution from experiment has been and have been sampled on prescribed days. At the end of the experiment a final pH measurement and analysis of the solution (ICP-OES) was conducted, as well as solid state analysis of the glass coupon, glass powder, and/or iron material. Solid state analysis will include, but may not be limited to, EPMA, XRD, and Raman.

These experiments are still in progress and will be terminated in December 2015.

7 Pressurized Unsaturated Flow (PUF) corrosion experiments

The work described in this section will be written for submission to a peer-review journal.

7.1 Introduction

We conducted a variety of glass alteration tests on glasses in pure water. These tests can be categorized into two types: 1. the static methods, and 2. the flow-through methods. Although both types have been applied to the measurement of glass corrosion rates, flow-through methods are the most adequate for the evaluation of the dissolution kinetics. This is due to the fact that the flow-through methods can easily provide a controlled and constant solution condition over the duration of the test. The downside to the use of these methods is that they require access to specialized equipment, and most experiments are run from 3-9 months. An example of a flow-through method is the single pass flow-through (SPFT) method (ASTM C1662 – 10). SPFT has been extensively applied to the measurement of the glass dissolution rate under variable environmental conditions. Setup for this method is straight-forward: powdered glass of a specific particle size or a glass monolith of known surface area is packed in a reaction cell at a high S/V (glass surface area to solution volume) ratio. The solution and reaction cell is then heated to a constant temperature (the protocol requires it to be below 100˚C), and the solution is introduced to the cell at a set flow rate. Aliquots of reacted solution are collected in set time intervals. This is usually done every 3 days, however more frequent sampling may be necessary at the beginning of the experiment if one wishes to determine the initial rate of corrosion of the sample. The effluent from the cells are preserved with a weak nitric acid solution, and analyzed by ICP-OES to determine the type and quantity of dissolved species in solution. At the completion of the experiment the cell is carefully unpacked and the solid material is analyzed with SEM and XRD.

A special kind of SPFT apparatus that is available at PNNL is the Pressurized Unsaturated Flow (PUF) system. The PUF system and test procedure have been described previously in the literature, [11,12,13,14] and only a general description is provided here. It is designed to simulate the open-flow and transport properties of the disposal system environment, while allowing the corroding glass to achieve a final reaction state. This method provides information on: A. the alteration phase or phases that form as a result of accelerated weathering, B. the evolution in the solution chemistry that occurs as a result of the glass-water interaction, which allows for model validation and direct determination of the corrosion rate, and c. glass-water reaction under hydraulically unsaturated conditions similar to those expected in a disposal-system environment. The information obtained from conducting PUF tests is a critical component for quantifying the long-term durability of and radionuclide release from glass or any other waste form after disposal. Preliminary PUF experiments have been completed at PNNL with pure deionized water and powdered ISG.

7.2 Experimental

Temperature	90°C
Glass form	Powder 40-60 mesh
Flow rate	4 mL·d^{-1}
Solution composition	18.2 MΩ·cm water
pH	Free, initially neutral
Duration	PUF, 200 days

Table 6. Summary of experimental conditions for alteration of ISG in saturated MgO solution.

Crushed ISG was prepared following the directions stated in ASTM C1662. The glass was crushed in a tungsten carbide mill and sieved to 40-60 mesh. The crushed material was then washed in ethanol by ultrasonication to remove any fines from the surface of the particles. The final material was dried to a final weight in a 90˚C oven. Three reprehensive samples of the glass was then studied and measured by SEM to verify that the size of the glass grains was consistent with the sieve size. The specific surface area of the crushed glass was 67605.6 m^2/g. This surface area was determined geometrically with the assumption that the particles were spheres with diameters equal to the average sieve size (equation (6)).

$$S_{\text{geo}} = \frac{3}{\rho r} \tag{9}$$

The PUF column, fabricated from chemically inert polyetheretherketone (PEEK), was packed with the previously prepared glass in intervals; the final total sample mass was 33.42 grams. The initial porosity of the column was determined to be 0.66. A porous Ti plate with a nominal pore size of 0.2 μm was sealed in the bottom of the column to provide an adequate pressure differential for the conducting of fluid while operating under unsaturated conditions[15]. The Ti plate was water-saturated prior to beginning the experiment and a small pressure was applied to interior of the column over the course of the experiment so as to only allow water to flow through the plate's pores. A glass pH electrode was calibrated at the beginning of the experiment at 4, 7, and 10, and the temperature probe was calibrated with boiling water (100˚C). The PUF experiment was allowed to run for 200 days at the nominal DIW (18 MΩ·cm) flow rate of 4.0 mL·d^{-1} at approximately 90˚C. pH, solution conductivity, column pressure, sample weight, and temperature data was collected on in-house software (LabView). A sample of the eluting fluid was collected every few days. These solutions were acidified with 2% nitric acid prior to being placed in cold storage.

7.3 Results

ICP-OES analysis of the solutions was completed just prior to the halfway point and at the end of the experiment. The change in the pH of the eluting solutions as a function of time is shown in **Figure 18**, and the normalized rate of reactions for each sampling are displayed in **Figure 19**. The rate of reaction was calculated using the equation below.

$$r_i = \frac{4\varepsilon Q \cdot NC_i}{\theta s(1-\varepsilon)\rho\pi d^2 L} \tag{10}$$

XRD, an example of which is shown in **Figure 20**, and SEM analysis of 18 sequentially removed subsections of the glass material was conducted to determine whether or not any crystalline or semi-crystalline products had formed on the surface of the glass.

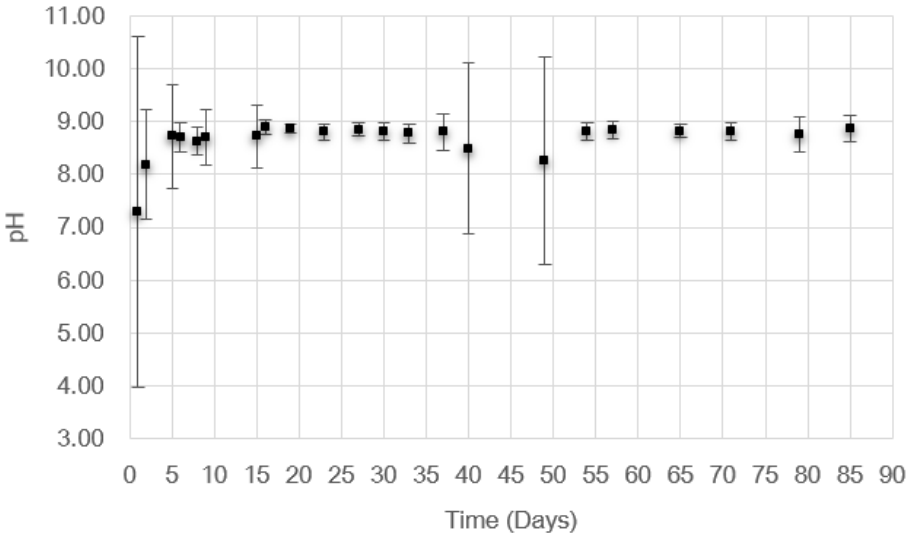

Figure 18: pH of the interacting solution was measured continuously over the course of the experiments. Preliminary analysis of the pH data suggests that the glass reached stage II within the 8-10 days of the start of the experiment

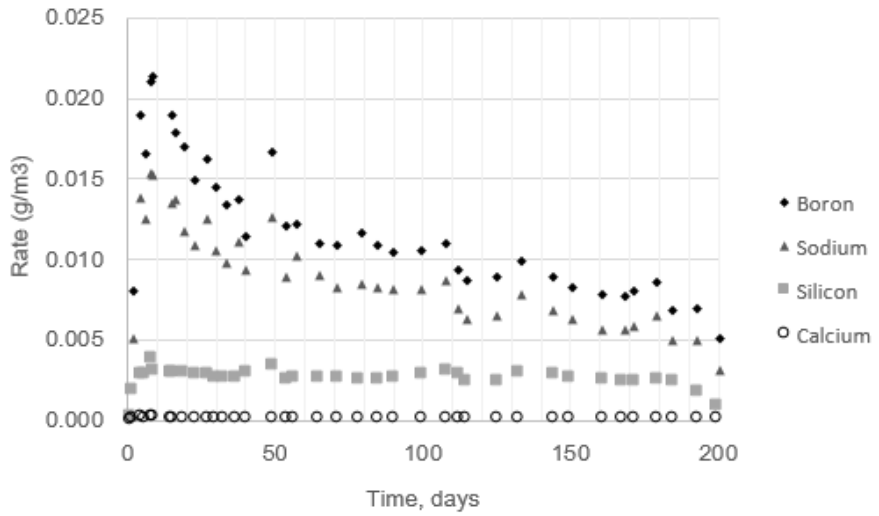

Figure 19: Samples of the eluting solution were collected every few days. Preliminary analysis of the data supports the observation that the glass reached stage II alteration within the first 10 days of the experiment

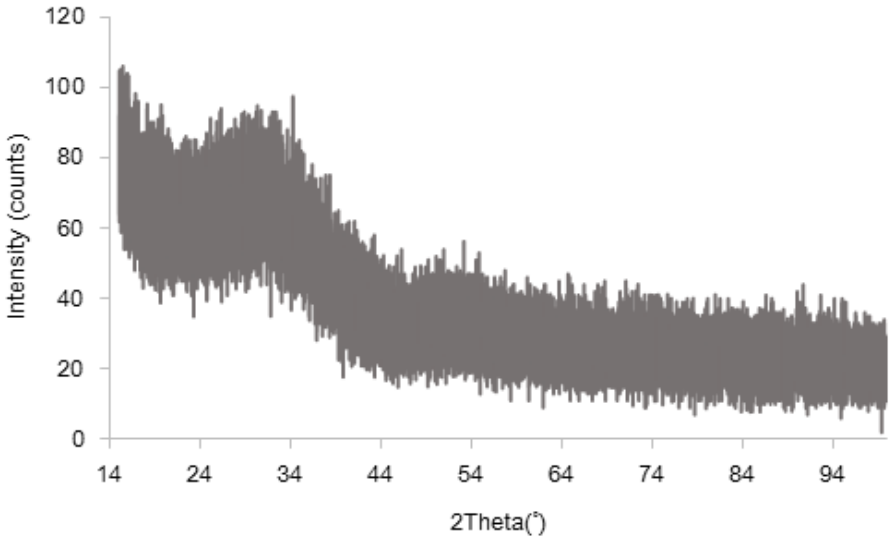

Figure 20: XRD analysis of subsection 6 to 18 of the glass removed from the PUF column. All 18 sections of the column appear to be amorphous and no crystalline products were detected.

7.4 Discussion

Preliminary analysis of the pH and ICP-OES data suggests that the glass most likely reached stage II dissolution at approximately day 8-10 of the experiment (**Figure 18**, **Figure 19**). There

is no indication that the glass ever reached stage III. XRD and SEM analysis of the subsections of the column has shown that no crystalline products formed on the surface of glass.

7.5 Future work

A second PUF experiment with ISG and iron powder was initiated in the Spring of 2015. This experiment is still underway and will be terminated in September/October of this year.

8 Glass Corrosion in the Presence of Iron-Bearing Materials and Potential Corrosion Suppressors

This work was published as "Glass corrosion in the presence of iron-bearing materials and potential corrosion suppressors" Joelle Reiser, Lindsey Neill, Benjamin Parruzot, Jamie Weaver, Christopher Musa, James Neeway, Joseph Ryan, Nikolla Qafoku, Stéphane Gin, Nathalie A. Wall. *MRS Proceedings 1744(Scientific Basis for Nuclear Waste Management XXXVIII), 1-6. **(2015)** DOI:10.1557/opl.2015.503*

8.1 Experimental

8.1.1 Materials

International Simple Glass (ISG) has a density of 2.5 $g \cdot cm^{-3}$ and a composition in weight percentages as follows: SiO_2: 56.2%, B_2O_3: 17.3%, Na_2O: 12.2%, Al_2O_3: 6.1%, CaO: 5.0% and ZrO_2: 3.3%.[3] The glass was obtained in bar form from Savannah River National Laboratory. Coupons were cut with a low-speed saw with a diamond tipped blade (Buehler Isomet®). The coupons were polished on a Leco Grinding and Polishing® SS-200 polisher up to 1200 grit. Dimensions of each coupon were approximately 10 × 20 × 2 mm^3. Hematite coupons (Fisher®) were cut to the same dimensions as the glass coupons and polished to 320 to 600 grit. Fe^0 foil (Sigma Aldrich®) of thickness 0.1 mm was cut to two of the same dimensions as the coupons 10 × 20 mm^2. Diatomaceous earth (DE) (MP-Biomedicals®) and fumed silica (SiO_2, called FS hereafter) (Sigma Aldrich®) were prepared as powders; DE was sieved to 149 – 250 μm, and FS was available at 0.2 – 0.3 μm. Deionized distilled water (18 MΩ) (DIW) was used.

8.1.2 Assembly Description

Figure 21 presents the experimental setups, which allows for determination of ISG corrosion in the presence of iron sources and as a function of the distance between the iron source and glass (both 0 mm – i.e. full contact – and 5 mm). Previous studies showed the importance of a complete contact between the iron source and the glass coupons, which allows for uniform glass corrosion.[16] In the present work, Fe^0 foil was etched with a knife in a grid pattern to facilitate solution flow between ISG and the Fe^0 $_{foil}$. The etched Fe^0 foil was flattened with a metal roller onto the ISG coupon, and the polished hematite coupon was pressed against the ISG surface. The gap between the two ISG coupons was maintained by 5 mm Teflon® spacers, and the sample configurations were held together with chemically inert glue (Loctite® Plastics Bonding System). Solution was allowed to flow along every surface of the glass except the portions touching the Teflon® blocks. Additional Teflon® spacers were used to elevate the bottom ISG coupon from the experimental stainless steel vessel (50 mL Parr®). The efficacy of glass corrosion suppressant (CS) – DE or FS – in the presence of Fe^0 was tested. The CS was placed in a bag made of 30 micron nylon mesh (Industrial Netting®) between the Fe^0 foil and the top ISG coupon, while the bottom ISG coupon remained out of contact with the CS. Solution was allowed to flow through the mesh bag to allow for every glass surface to be in contact with solution with the exception of portions in contact with the Teflon® blocks. Additionally, blank samples were prepared: Teflon® blocks and glue; ISG with Teflon® blocks and glue; FS with Teflon® blocks and glue, DE with Teflon® blocks and glue; ISG with DE, Teflon® blocks, and glue; and ISG with FS, Teflon® blocks, and glue. The following nomenclature is used to designate experimental setups: ISG/iron source/CS (e.g. ISG/Fe/DE means ISG alteration in the

presence of Fe^0 and DE, ø indicates the absence of iron source or CS). Each sample set was prepared in duplicates for statistical analysis.

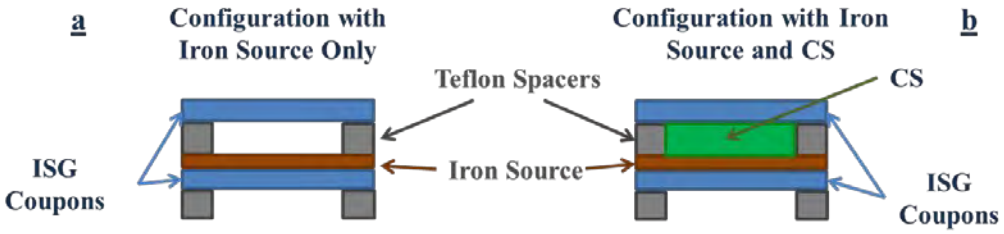

Figure 21: Schematic Representation of the Experimental Configurations with a) Iron Source Only and b) Iron Source and Corrosion Suppressant (CS)

Each configuration was inserted into Parr® vessels containing 25 mL DIW to obtain a glass-surface-area-to-solution-volume ratio (S/V) of 40 m^{-1} with the exception of ISG/ø/ø which had an S/V of 20 m^{-1}. The solutions were purged with pure N_2 (A-L Compressed Gases, Inc.) and solution pH was measured at room temperature before sealing the Parr® vessels. All experiments were carried out in a 90°C oven for 1 month without disturbing the samples. Losses due to evaporation were negligible. The solutions were then removed and pH was measured at room temperature. Glass samples were washed with ethanol and dried in a desiccator. ISG samples were then cut for various analyses.

Characterization Techniques

Solutions were diluted with 1-2% HNO_3 and analyzed using Inductively Coupled Plasma Optical Emission Spectrometry (ICP-OES) (Perkin Elmer® Optima 3200 RL) for Al, B, Ca, Fe, Na, and Si; the instrument was calibrated using dilutions of standard solutions (Inorganic Ventures).

Normalized loss (NL_x) of B, Si, and Na from ISG in $g \cdot m^{-2}$ was calculated using the following equation:

$$NL_x = \frac{C_X}{\left(\frac{S}{V}\right) f_X} \quad (11)$$

Where C_X is the elemental concentration in $g \cdot m^{-3}$, f_X is the mass fraction of the selected element in ISG, and S/V in m^{-1}. NL(Si) is corrected for excess Si for samples that contained fumed silica, based on Si concentration determined in ø/ø/FS configurations. This correction is calculated from the Si release of a sample of fumed silica altered in water for one month. This correction could not be applied to the samples containing DE due to experimental error associated with the Si concentration for the ø//ø/DE blank.

Altered monoliths were embedded in epoxy resin (Specifix-20®) polished to 1200 grit and sectioned to expose the cross section. Altered and unaltered glass compositions were measured by Energy-Dispersive X-ray Spectrometry (EDS) using the JEOL JXA-8500F electron microprobe, equipped with a Thermo Scientific UltraDry EDS detector and ThermoNORAN™ System 7 analytical software. Measurements were made using an accelerating voltage of 15 kV, and a beam current of 8 nA. The beam was defocused to a 1µm spot size to help mitigate alkali migration under beam irradiation.[17] Due to the roughness of the surfaces, quantitative data could not yet be obtained from EDS analyses. The thickness of the alteration layer was measured using

the SEM images of the cross sections and ImageJ software. Alteration layer thickness was measured at multiple points on a glass side to allow for statistical analysis.

8.2 Discussion

Over the course of the experiment, sample solution pH increased from a range of 5.0 - 6.0 to 7.5 - 9.5. **Figure 22** shows NL_x for B, Na, and Si. Uncertainty is reported as twice the standard deviation associated with results obtained from duplicate analyses. Boron is used as a tracer of glass alteration because B is known to not be retained in the alteration products. NL(B) and NL(Na) are comparable for most samples for the chosen S/V of 40 m^{-1}. NL(Si) is smaller than NL(B) and NL(Na) for each sample; NL(Si) is particularly small for ISG/Fe/ø. In general, samples featuring corrosion suppressants, FS or DE, have lower NL(B) than their counterparts in absence of FS or DE, indicating that corrosion suppression is occuring. However, there is no statistical difference between NL(B) values for ISG/Fe/ø and ISG/Fe/FS. At this point, FS is not known to be an appropiate suppressant for ISG corrosion in the presence of Fe^0. NL(B) is slightly smaller for ISG/Fe/DE than for ISG/Fe/FS.

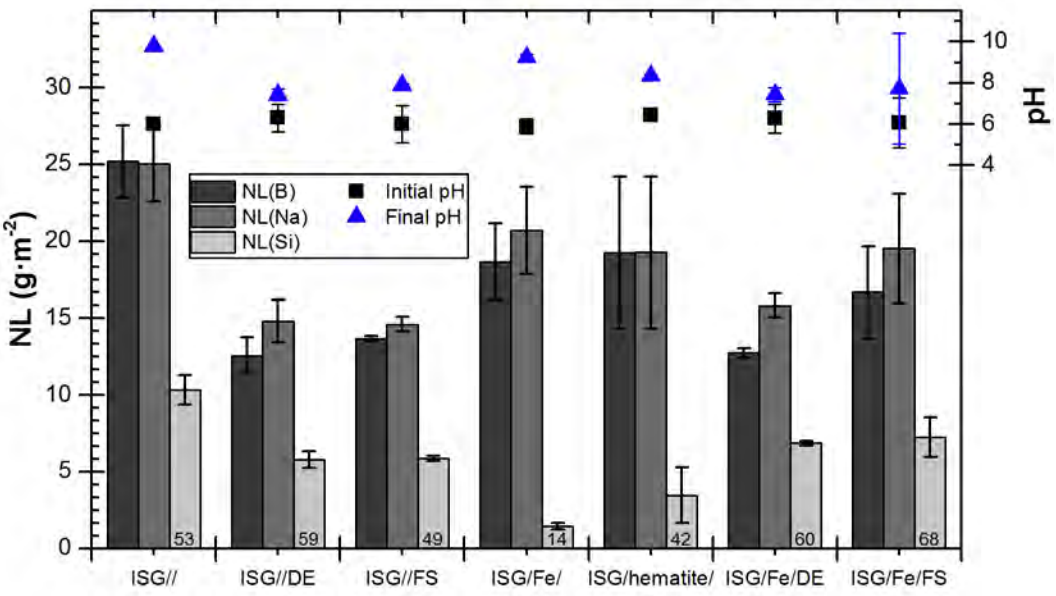

Figure 22. Normalized mass losses (NL_x) for each sample calculated from solution concentrations of B, Na, and Si (left axis), initial and final solution pH (right axis), and corrected concentrations of Si in ppm shown in the NL(Si) bars

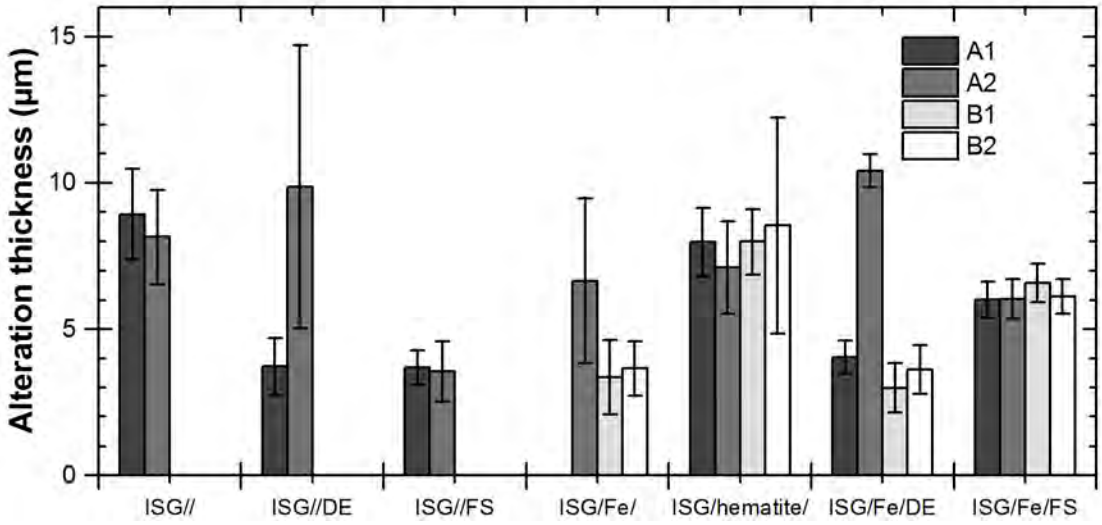

Figure 23. Alteration thickness measurements obtained from SEM cross sections of altered coupons. The labels indicate the identity of the glass coupon and its side and refer to the drawing, with A1 being the top side of the upper glass coupon, for example. SEM micrographs will be provided in another manuscript.

The alteration layer thicknesses of the various surfaces are shown in **Figure 23**; alteration layers were not observed on all surfaces because the layers were too thin. Additionally, the surface in contact with iron (B1) in ISG/Fe/DE, ISG/Fe/FS, and ISG/Fe/ø configurations had alteration layers that contained iron as indicated by EDS spectra. A2 alteration layers did not contain iron, but secondary products featuring trace levels of iron were observed at the surface of the altered glass coupon. Within a single sample, alteration layer thicknesses are not identical within reported uncertainty for ISG/ø/DE (A1 and A2) and ISG/Fe/DE (A2 versus all the other coupon sides). For all the other samples, alteration thicknesses do not vary between glass coupon sides. However, for the surface of the top coupon in contact with the mesh bag that contains the CS, the alteration thickness is larger for ISG/Fe/FS than for ISG/Fe/DE for surfaces B1 and B2, and the alteration thickness is larger for ISG/hematite/ø than for ISG/Fe/ø. Comparison between ISG/ø/ø and ISG/Fe/ø shows no statistical difference between their results at A2, indicating that the upper coupon is too far from the Fe source for Fe to influence alteration.

NL_x values determined from solution analysis can be converted to an equivalent altered glass thickness based on the density of ISG. This equivalent altered glass thickness is an average value over the whole glass surface area, S, and can thus be compared to the average of the 4 alteration layer thicknesses obtained from solid state analysis measurements (A1, A2, B1 and B2). **Figure 24** shows the comparison of alteration layer thickness from solution and solid state analysis. The dashed columns on **Figure 24** represent configurations that featured Fe in the some alteration layers. For configurations ISG/ø/ø, ISG/ø/DE, ISG/Fe/DE, and ISG/Fe/FS, the calculated solution and measured solid alteration thicknesses are statistically equivalent.

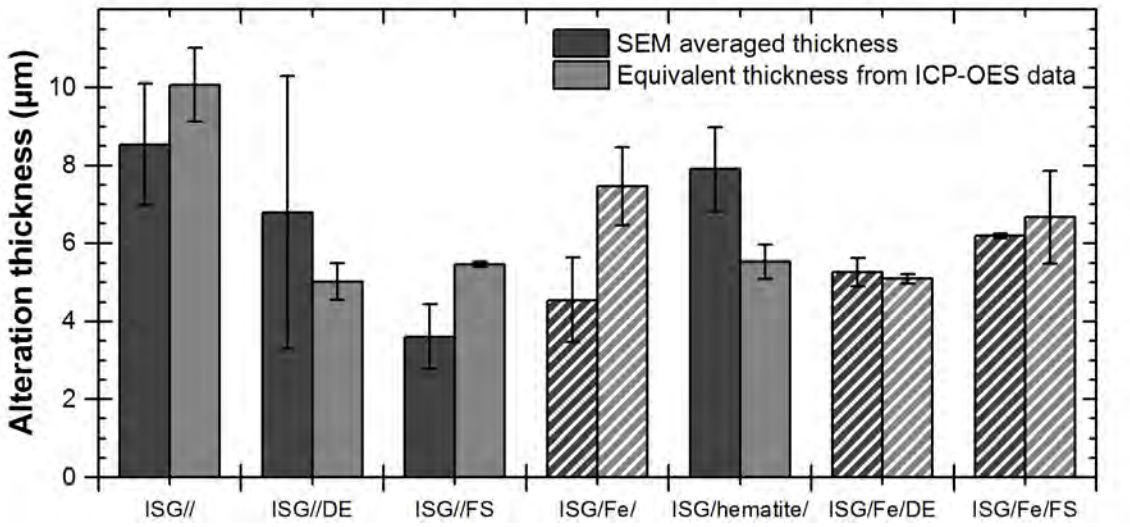

Figure 24. Alteration Thickness Comparison. Dashed columns: presence of Fe in some alteration layers.

The alteration thickness for ISG/Fe/ø measured by SEM is statistically smaller than the thickness determined from solution data; this may be due to calculation artifacts that do not account for the fact that the presence of Fe in the alteration layer increases the layer density. The differences between the resulting alteration thicknesses for ISG/hematite/ø can be due to an excessive amount of glue on the surface of the coupons that reduced the glass surface area in contact with water. The apparent differences observed for the ISG/ø/FS alteration thicknesses deducted from either solution or solid analysis will be investigated further with additional long-term experiments.

8.3 Conclusions

Results presented in this paper are preliminary data for further work, in which similar glass corrosion tests will be run for longer time periods and the distance between upper glass coupons and Fe sources will be decreased. Additionally, the phases into which Fe is incorporated in the alteration layer will be investigated.

9 Wet Chemical and UV-Vis Spectrometric Iron Speciation in Low and Intermediate Level Nuclear Waste Glasses

This section was published as "Wet Chemical and UV-Vis Spectrometric Iron Speciation in Low and Intermediate Level Nuclear Waste Glasses". Jamie L. Weaver, Nathalie A. Wall, John S. McCloy. *MRS Proceedings - 1744(Scientific Basis for Nuclear Waste Management XXXVIII), 1-8* ***2015)****DOI:10.1557/opl.2015.481*

9.1 Introduction

In the United States, nuclear waste glass (NWG) is primarily based on alumino-boro-silicate glass compositions, chosen for their ability to incorporate a variety of elements, including various multivalent elements potentially present in the nuclear waste slated to be vitrified at the Hanford site in Richland, WA.[18] Of these elements, iron has been found to play an important role in defining the efficiency of the vitrification process, the structure of the glassy matrix, and the long-term durability of the final glasses. Iron present in glass can be found as a mixture of ferrous or ferric cations.[19] Previous studies have shown that an Fe oxidation state ratio Fe(II)/Fe(III) between 0.1 to 0.5 is ideal for melting conditions.[19,20]

In recent years this Fe(II)/Fe(III) ratio and the total iron content in glass has been studied by Mössbauer, Raman, XANES, and optical spectroscopy methods.[21,22,23] The first three techniques listed above require access to expensive (both in terms of time and money) and, in the case of XANES, highly specialized equipment which may not be readily available for the quick analysis of simulate nuclear waste glasses. However, optical spectroscopy equipment is comparatively inexpensive, relatively quick to execute, and data analysis is straight forward. A plethora of destructive and non-destructive optical spectroscopy procedures have been published for the analysis of iron in glass, providing a strong foundation on which to build new protocols.[24,25,26] This study presents a revised experimental protocol that has been assimilated from the previously referenced sources. It also reports difficulties that were encountered during the utilizing wet chemistry methods coupled with UV-Visible spectroscopy to determine the Fe(II)/Fe(III) ratios and total iron content of quenched and non-quenched alkali alumino-boro-silicate, representative of nuclear waste glasses.[24]

9.2 Experimental

A Cary 5000 (Agilent) UV-Vis NIR Spectrophotometry was utilized in this study, and data was analyzed with the Cary WinUV software. All samples were measured in transmission mode (%T) at 520 nm in 1 cm plastic cuvettes, and referenced to 18 MΩ deionized distilled water (DDIW) at ambient temperature (ca. 20˚C). Standard solutions and glass sample analyses were run in triplicate.

The simulated NWGs used in this study are described in Table 1 and were provided by collaborators at the Pacific Northwest National Laboratory in Richland, WA. The glasses were batched and melted using metal oxides and other typical precursors (e.g., carbonates, boric acid).

After batching, each glass was mixed in an agate mill for approximately 3 minutes and then placed into a platinum crucible (Pt/10%Rh) and melted for 1 hour at 1150 - 1400°C, depending on the composition. The resulting glasses were air-quenched by pouring the melt onto a stainless steel plate. Undissolved solids were noted in the glasses after the cooling period ended. To increase the homogeneity, the glass from the first melt was ground to a powder in a tungsten carbide mill (4 minutes, Angstrom Inc.), and melted a second time at the same or slightly lower temperature than the first melt. All the glasses were subsequently air-quenched. The resulting glasses had a uniform appearance upon cooling, and no undissolved solids were observed. The glasses were heat-treated in accordance with the standard CCC procedure for the Hanford Waste Treatment & Immobilization Plant.[27] The final color of the glasses ranged from dark green to dark brown. Finally, the glasses were ground and sieved to a 100 mesh diameter (149 micrometers). Before wet digestion of the glass, each powdered sample was placed on a bench top vortex mixer for 2 minutes. It was determined over the course of this study that omission of this step led to inconsistent Fe intensities for replicate samples.

UV-Visible spectrophotometry calibration was established using a set of 5 standard iron solutions prepared from solid ferrous ammonium sulfate hexahydrate (Sigma Aldrich): 0.07 g of the ferrous ammonium sulfate was weighed and transferred into a 1.00 L volumetric flask and diluted with 200 mL of DDIW; 3.00 mL of concentrated H_2SO_4 was added, and the resulting solution was diluted with additional DDIW to reach 1 L. From this stock 0, 0.1, 0.5, 1.0, 2.0, 3.0 and 5.0 wt % standard iron solutions were prepared. These standard solutions were found to be valid for 24 hrs, after which time the color of the solutions would begin to degrade. Thus, the calibration curves and experimental data must be measured within the same day.

50.000 mg of glass was weighed into a 100 mL Teflon beaker, and ~0.50 mL of H_2SO_4 and ~1.00 mL 48 to 51% HF (Sigma Aldrich) were added. The mixture was carefully swirled until all particles dissolved into solution. Once the solution had cooled, it was then diluted by a factor of 10 with DDIW and well mixed. Using a plastic pipette, 2.0 mL of the solution was transferred to another 100 mL Teflon beaker, and mixed with an addition of 25 mL of DDIW. An ammonium acetate buffer solution was then used adjust the pH of the solution to 3.4 ± 0.01 and 5.00 mL of 1,10 phenanthroline solution was added to the beaker and then diluted to 50 mL with DDIW. 1,10 phenanthroline ($C_{12}H_8N_2$, ortho-phenanthroline or o-Phen, Sigma Aldrich) is a tri-cyclic nitrogen heterocyclic compound that reacts with Fe^{2+} to form a stable and brilliant red colored complex.

At the beginning of this study it was found that the ratio of HF/H_2SO_4 needed to dissolve the powdered material varied from glass to glass, and that an excess of HF present in solution made it difficult to accurately buffer and dilute our solutions to the desired final volume. Therefore, prior to dissolution of any of the glasses, a set of trial dissolutions were conducted to determine the appropriate ratio of acids needed to dissolve the glass, and the approximate volume of buffer solution required to raise the pH of the solutions to 3.4. The addition of this step improves the overall reproducibility of our experiments.

Ammonium acetate buffer was prepared by dissolving 250.0 mg of ammonium acetate to 150 mL with DDIW and adding 700 mL of glacial acetic acid. The 1, 10 - phenanthroline solution was prepared by dissolving 100 mg of 1, 10 phenanthroline monohydrate (Sigma Aldrich) to 100 mL with DDIW, and we added a few drops of HCl to hasten dissolution. Although not stated in previous protocols we determined that it was necessary to wait 5 minutes before transferring a portion of the solution to a 1 cm plastic cuvette for analysis. Waiting more or less than 5 minutes led to variability in the %T measurement. For this solution %T was measured three consecutive times. Within 30 minutes of the first measurement, exactly 30 mg of hydroxylamine HCl crystals (a mild reducing agent) were added to the remainder of the sample, which was placed on at hot plate at 90˚C for no more than 4 minutes, and the solution was allowed to cool to room temperature for 12 hours. It was found that allowing the solution to heat longer than 4 minutes, or at a temperature higher than 90 ˚C lead to inconsistent color development in the final product. The resulting solution was transferred into a clean cuvette and the %T was again measured in triplicate. Total ferric ion concentration was calculated by subtracting the experimentally determined total iron concentration from the ferrous iron concentration.

9.3 Discussion

Iron redox analysis results on the simulated NWG glasses are shown in **Table 7**. The calculated total amount of iron (ug) for each glass was in good agreement with the target compositions, albeit slightly smaller.[27] This may be due to the presence of interfering ions in solution that also complex with 1,10 phenanthroline, therefore reducing the total amount of ligand available with which iron could bind.[28] Using citrate in place of ammonium acetate as a buffer will be the subject of future research with glass of compositions similar to those studied in this method. Another source of error in the iron measurements can be attributed to inconsistent sampling when the glass was powdered. All glasses analyzed showed a Fe(II) /Fe(III) ratio between 0.06 and 0.04 with an average standard deviation of approximately ± 0.01 wt%. These values are consistent with that obtained for similar glass compositions melted under similar conditions, indicating ~94 – 96% Fe (III) ions.[29,30] Additionally, it is possible that our Fe(II) results are slightly higher than what may be expect due to the processing of the glass in a tungsten carbide mill.

Table 7. Experimentally determination of Fe(II)/Fe(III) ratios in HLW glasses. All reported values are the average Fe ion in ug, and they are reported to three standard deviations from the mean of triplicate samples.

Glass	Fe (II)	Fe_{total}	Fe (III)	Fe(II)/Fe(III)
HLW-E-ANa-13(3Al-3Si)	0.16 (±0.04)	2.46 (±0.08)	2.30 (±0.06)	0.06 (±0.02)
HLW-E-ANa-24	0.12 (±0.04)	2.54 (±0.09)	2.42 (±0.11)	0.05 (±0.01)
HLW-E-ANa-25	0.10 (±0.03)	2.83 (±0.23)	2.73 (±0.25)	0.04 (±0.01)
HLW-E-ANa-26	0.10 (±0.05)	2.53 (±0.06)	2.43 (±0.09)	0.04 (±0.02)
IWL-HAC5-1	0.12 (±0.04)	2.58 (±0.14)	2.46 (±0.18)	0.05 (±0.02)

9.4 Conclusion

In the assessment of the process and material produced from the vitrification of nuclear waste it is necessary to know the ratio of valence states of elements in the glass matrix. Many methods currently used are time consuming and require the use of expensive and specialized instrumentation. UV-vis spectroscopy is an exception to these cases, and has been shown to be an effective and quantitative method by which to determine the ratio of Fe(II)/Fe(III) in simulated nuclear waste glasses. With the substitution of a suitable ligand, and adjustments to the pH range of experiment it may be possible to modify the above described procedure for the analysis of other multivalent species in simulated nuclear waste glasses.

10 A Sampling Method for Semi-Quantitative and Quantitative Electron Microprobe Analysis of Glass Surfaces

This section was published as "A Sampling Method for Semi-Quantitative and Quantitative Electron Microprobe Analysis of Glass Surfaces". Jamie L. Weaver, Joelle Reiser, Owen K. Neill, John S. McCloy, Nathalie A. Wall. *MRS Proceedings 1744(Scientific Basis for Nuclear Waste Management XXXVIII), 1-6* ***(2015)*** *DOI:10.1557/opl.2015.496*

10.1 Introduction

Energy Dispersive Spectroscopy-Electron Probe Micro Analysis (EDS-EPMA) is a common method used to analyze corroded glass surfaces. In the past EDS-EPMA has been used to identify the presence of a hydrated and silica-rich alteration layer and the formation of solid composites on the glass surface.[31,32,33] EDS allows the user to obtain clear and detailed images of the corroded surface morphology over large area (μm^2), and to characterize the element(s) involved in the glass corrosion process. Glass studies often couple EPMA with Induction Coupled Plasma – Optical Emission Spectrometry (ICP-OES) to determine glass corrosion rate, and to attempt definition of glass corrosion mechanisms.[1,34,35] Most of these studies utilize "standardless" EDS, a method that suffers from both accuracy and precision limitations, especially in comparison to wavelength-dispersive X-ray spectroscopy (WDS).[36] This form of EDS is sufficient to detect the gross chemical variations caused by the alteration processes, such as complete loss of Na in the altered layers, but cannot accurately quantify the amount of loss. ICP-OES data is used to fill in this information. However, in situations when it is not possible to obtain or analyze a sample of the corroding solution, analysis of a corroded surface by EPMA becomes more important, and more rigorous methods are required.

One such method is "standard" based EDS, which is semi-quantitative. In this method an unaltered sample of the glass is measured with the corroded samples under the same analysis conditions, and then the calculated elemental weight percent's (wt%) of the altered glasses are compared to those of the unaltered glass. A second method that can be used is standard based WDS. The setup for this form of analysis is similar to that used for the standard based EDS method, but it includes an additional calibration setup that compares the X-ray intensities collected from the unaltered and corroded glasses to a set of standard samples. In this study both methods were executed on sets of unaltered and altered glass samples. The sets of samples were measured in a planar orientation, and in cross-section.

10.2 Experimental

International Simple Glass (ISG was chosen for this study due to its relatively simple oxide composition (**Table 8**). A 50 kg ISG sample was produced in May 2012 by MoSCI Corporation (Rolla, MO) and subsequently divided into 500 g glass ingots.[4] The glass ingot used in this study was cut into coupons with an oil (IsoCut™ Fluid, Buehler) lubricated diamond saw (IsoMet™ Low Speed Saw, Buehler). Approximate dimensions of the coupons were 30 mm × 10 mm × 4 mm. Each coupon was

Element	Wt%
Si	56.20
B	5.37
Na	9.05
Al	3.23
Ca	3.57
Zr	2.44

Table 8. ISG elemental composition by weight percent.[1]

polished at 120, 320, 600, and 1200 grits using an oil-based lubricant (IsoCut™ Fluid, Buehler) on a Leco Grinding and Polishing Polisher.

Table 9 lists the type of EPMA analysis used on each sample. The $MgCl_2$ and water corroded samples were prepared in the following manner: ISG coupons were prepared in the above described way and then subjected to 7 day Product Consistency Tests (PCT) as defined in ASTM C1285.[37] These tests were conducted at 90˚C in distilled deionized water (18MΩ) or saturated $MgCl_2$ solution. The surface area/volume value for these samples was 2.5 (± 0.1) cm^3/mL solution. At the end of the test the samples were carefully removed from the corroding solution and dried under ambient conditions for 48 hours before being placed in a desiccator for storage.

Coupons designated to be measured in planar orientation were lightly coated with a layer of carbon and grounded to the sample holder prior to being placed in the EPMA. The unaltered coupons to be measured in the planar orientation were oil polished with 6 μm diamond paste prior to being carbon coated. Coupons chosen to be measured in cross-section were first diagonally cut with a tungsten carbide blade, placed on end in ~2 mL of Specifix-20 resin, and allowed to try for 20 to 24 hours. The cross-sectioned surface was then polished to a smooth using 9 μm diamond paste (Ted Pella), and then carbon coated and grounded to the sample holder with carbon tape.

All EPMA analyses were conducted using the JEOL JXA-8500F electron microprobe at the Peter Hooper GeoAnalytical Lab of the WSU School of the Environment, equipped with 5 WDS spectrometers, a Thermo Scientific UltraDry EDS spectrometer, ProbeForEPMA WDS automation and analytical software for WDS analyses, and ThermoNSS System7 automation and analytical software for EDS analyses. EDS measurements were made using an accelerating voltage of 15 kV, and a beam current of 8 nA. The beam was defocused to a 1 μm spot size to help mitigate alkali migration under beam irradiation. EDS spectra were collected for a total of 60 live-time seconds. Elemental concentrations from these measurements were determined from raw EDS intensities using the PROZA ϕ(ρz) matrix correction, similar to that outlined in Bastin and Heijligers, through the ThermoNSS System 7 software package.[38]

Sample	Unaltered, planar orientation	Corroded with $MgCl_2$, Planar orientation	Corroded with H_2O, Planar orientation	Unaltered, cross-section orientation
Analyses Type	EDS/WDS	EDS	EDS	EDS/WDS

Table 9. Type of analyses (EDS or WDS) and samples analyzed

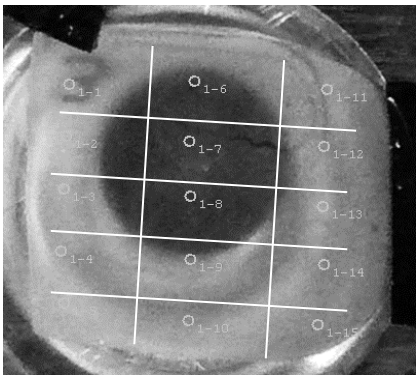

Figure 25. Grid overlaid on uncorroded planar oriented ISG glass coupon. The red marks show the approximate areas where EDS and WDS measurements were acquired on the surface.

WDS measurements were made using an accelerating voltage of 15 kV, a beam current of 6 nA, and a beam size of 10 μm. A list of peak and background counting times and calibration standards can be found in **Table 10**. Concentrations were determined from raw X-rays measured by WDS using a ZAF intensity correction (Armstrong-Love/Scott) through ProbeForEPMA analytical software.

Analysis of the planar surface of an unaltered ISG coupon was conducted by dividing the surface into a 3 x 5 grid (**Figure 25**). One data point was taken for each grid square for a total of fifteen points being collected per planar surface. Alternatively, the cross-sectioned surfaces were divided into 1 x 5 grid, and three data points were taken per each square. The total number of data points collected from the cross-sectioned surfaces was also fifteen. Although EPMA information was collected on all oxides in ISG, only three are discussed here. These three oxides were chosen because they are known to be leached during the corrosion of ISG.[3] Boron, an element commonly used to monitor the corrosion process, has been emitted from this list due to complications with measuring it with EPMA.[39]

Statistical analysis of the data was conducted using the Statistical Package for the Social Sciences (SPSS) Software 21 (IBM). Contrary to its name, SPSS is a powerful software package widely used in all scientific fields. Wt% data collected from EPMA analysis of all surfaces was imported into SPSS, and then group statistical tests (calculation of mean, standard deviation, and analysis and removal of outliers), Independent Samples T-tests, and Levene's Test for Equality of Variances. Statistical group analysis was completed for all measured surfaces. T-tests and Levene's Tests were conducted on the EDS and WDS measurements taken from the unaltered planar ISG sample and the unaltered cross-sectioned ISG sample. Levene's test values were calculated for each set of comparison, and were found to be significant for all *t*-tests.

Element	Peak Counting Time (s)	Low Background Counting Time (s)	High Background Counting Time (s)	Spectrometer #	Analyzing Crystal	Calibration Standard
SiO_2	20	10	10	4	PETJ	Kakanui Anorthoclase (USNM 133868)
Al_2O_3	15	7.5	7.5	1	TAP	ISG
Na_2O	15	7.5	7.5	1	TAP	Wilburforce Hornblende

Table 10. Details of WDS measurement conditions, including beam conditions, peak and background counting times and calibration standards

10.3 Discussion

Group statistical data for all EDS analyses are highlighted in **Table 11**. Measurement errors were calculated to two standard deviations. Calculated elemental wt% for corroded surfaces showed large errors as compared to the unaltered surfaces. This is most likely due to uneven corrosion across the surface of the coupons. The unaltered surfaces did not show as large of error values as the corroded surfaces, but t-test values show that their means differ significantly (**Table 11**). This was as unexpected result as it was assumed that the composition of the unaltered planar surface was the same as the unaltered cross-sectioned sample. The elemental wt% values were also not in good agreement with the theoretical wt% values for ISG (**Table 8**). To investigate whether this difference was the result of method error or from compositional differences between the two samples the two surfaces were measured with WDS.

WDS results show significantly less difference between the mean values measured for the two surfaces, and both values were in good agreement with theoretical wt% for each oxide. The

calculated errors for the WDS measurements were also smaller except in the case of SiO_2. Therefore, our two unaltered glass surfaces are statistically similar.

Oxide	Unaltered, planar orientation (*wt%*)	Corroded with $MgCl_2$, planar orientation (*wt%*)	Corroded with H_2O, planar orientation (*wt%*)	Unaltered, cross-section orientation (*wt%*)
Na_2O	10.6, *1.8*	2.0, *2.7*	1.79, *3.0*	5.0, *2.4*
A_2O_3	3.9, *0.2*	3.8, *1.9*	6.10, *2.2*	4.2, *0.6*
SiO_2	32.0, *1.0*	21.8, *14.5*	33.31, *2.3*	35.0, *1.0*

Table 11. Group statistics for samples measured by EDS. The first number listed is the mean of all point measured, and the *second number* is the error of the measurement (2σ, 95% confidence interval).

10.4 Conclusion

Standard based EDS analysis of the unaltered and corroded surfaces of a simulated nuclear waste glass has been shown to be able to detect gross chemical variations caused by the alteration processes. However, at this time, it cannot accurately quantify the amount of elements leached from a corroded glass surface. Elemental wt% calculated from standard based WDS analysis of two surfaces of unaltered glasses has been shown to be in good agreement with theoretical elemental wt% values. Additional research is being conducted to determine whether this method of WDS can be used to accurately determine the difference in elemental composition between a corroded an unaltered glass surface.

EDS		Planar Surface	Cross-Section	WDS		Planar Surface	Cross-Section
Na (wt%)	**mean**	10.6	5.0	**Na (wt%)**	**mean**	9.1	9.1
	σ	1.8	2.4		**σ**	0.1	0.2
	t-test	18.7			***t-test***	0.2	
	p	7.6			***p***	1.3	
	df	27			**df**	24	
Al (wt%)	**mean**	3.9	4.2	**Al (wt%)**	**mean**	3.3	3.3
	σ	0.2	0.6		**σ**	0.03	0.03
	t-test	-3.6			***t-test***	-0.6	
	p	6.3			***p***	0.9	
	df	27			**df**	24	
Si (wt%)	**mean**	32.0	35.0	**Si (wt%)**	**mean**	26.2	26.2
	σ	1.0	1.0		**σ**	0.1	0.1
	t-test	-21.8			***t-test***	1.0	
	p	7.6			***p***	0.1	
	df	27			**df**	24	

Table 12. Results of statistical analysis of WDS measurements of planar and cross-sectioned unaltered ISG surfaces. All error is reported to two standard deviations measurement (2σ, 95% confidence interval).

11 Corrosion of Saltstone and Cast Stone in the Presence of Various Groundwaters

11.1 Introduction

SRNL cement production begun in early 1990s, with cementation of 1.3×10^5 m^3 of waste (sludge and soluble salt supernate). France also uses cementation for the containment of sludges. Cementation offers the advantage of low cost and tailored composition; however, it leads to caustic leaching solutions. The composition of the samples studied, Castone and Salstone are presented in the table below.

	Cast Stone	Saltstone
Portland Cement Type I/II	8 %wt	10 %wt
Class F fly ash	45 %wt	45 %wt
Type 100 blast furnace slag	47 %wt	45 %wt
SiO_2	39.5	37.1
TiO_2	0.7	0.7
Al_2O_3	15.7	14.1
FeO	5.5	2.9
MnO	0.2	0.1
MgO	5.6	3.6
CaO	21.1	29.2
Na_2O	10.2	10.9
K_2O	1.1	1.0
P_2O_5	0.2	0.3
Traces > 100 ppm	Sr,Ba,Zr,V,Zn,Cr	Ba,Sr,Cr,Zr,Zn,Ni

Table 13. Cementitious waste form composition

Experiments to study Saltstone and Cast Stone alteration in various synthetic ground waters were initiated. The selected groundwaters are: deionized water, brine (5 M NaCl), lime groundwater, Boom Clay groundwater, Grimsel groundwater, Yucca Mountain groundwater (J-13), Savannah River Site groundwater (SRS), Hanford groundwater (PNNL), General Weep Brine (GWB), ERDA-6 (from WIPP) and 5 m NaCl, which main features are described in **Table 14** and actual compositions are detailed in **Table 15**.

Name	Geological context	Main Elements
Deionized Water (DIW)	-	-
Brine	(Salt formation)	Na, Cl
GWB ERDA-6	WIPP, Salt formation	Na, Cl, K, Mg Na, Cl
J-13	Yucca Moutain Test Site	Na, Mg, Ca, K
PNNL	Hanford subsurface groundwater	Ca, Na, Mg
Lime	Limestone	Ca
Boom Clay	Test site (France, Belgium)	Na, Mg, B, K
Grimsel	Test site (Switzerland)	Na, Mg, Ca, Si
SRS	Savannah River, subsurface groundwater	Na, Cl, Ca, Mg

Table 14. Synthetic groundwaters

boom clay		
	quantity (mg)	M
NaHCO3	1170	1.39E-02
H3BO3	43	6.95E-04
KCl	25	3.35E-04
MgCl2.6H2O	22	1.08E-04
NaF	11	2.62E-04
NaCl	10	1.71E-04
Na2SO4	0.3	2.11E-06
CaCO3		saturated
c. Bruggeman et al. 2005		

Synthetic Grimsel Groundwater Recipe		
Compound	g/L	g for 500mL
Na2SO4	0.144	0.072
KCl	0.0048	0.0024
MgCO3	0.0427	0.02135
NaHCO3	0.2733	0.13665
CaCl2	0.013	0.0065
H4SiO4	0.0341	0.01705
pH	8.6-8.8	
Kersting et al, 2012		

	GWB	ERDA-6
	g/L	g/L
Na2B4O7.10H2O	15.06	6
NaBr	2.74	1.13
LiCl	0.19	NA
NaCl	179.61	261.64
KCl	34.84	7.23
MgCl2.6H2O	207.05	3.86
CaCl2.2H2O	2.03	1.76
Na2SO4	25.23	23.7
Xiong 2008 (SP 20-4)		

J-13 groundwater recipe (yucca mtn)	
reagent	quantity @ 60C g/L
NaHCO3	128.45
NaF	3.1826
Na2SO4	12.2364
Na2SiO3.5H2O	0.204
MgSO4.7H2O	21.392
CaCl2.2H2O	7.598
Ca(NO3)2.4H2O	12.1685
HCl	0.00373
KCl	6.4178
KHCO3	0.0104
CaCO3	37.1173
H2SO4	0.0893
Gdowski, 1997	

PNNL groundwater recipe (email from Jim) Vadose Zone Pore Water Recipe		
Order to dissolve	Reagents Available	g/L
1	CaSO4•2H2O	2.0661
2	NaCl	0.0994
3	NaHCO3	0.0336
4	NaNO3	0.289
5	MgSO4	0.313
6	MgCl2•6H2O	0.4879
7	KCl	0.0522
Adjust pH to 7.0 to 7.2 with sodium hydroxide or sulfuric acid.		

SRS subsurface groundwater conditions	
	mg/L
Na	1.39
K	0.21
Ca	1
Mg	0.66
Cl	5.51
SO4	0.73
pH	5
Seaman et al, 2013	

Table 15. Synthetic groundwaters detailed composition

The experimental setup is shown with **Figure 26**. The samples were run in duplicate and placed in an oven set to 90°C for 1 month with 79-150 µm powder. The pH and solutions were monitored at days 0, 1, 3, 9, 21, and 30 to determine initial rates. ICP-OES analyses were performed on the solutions for quantification of Si, Al, Na, K, Ca, Cr. Powders were analyzed by SEM.

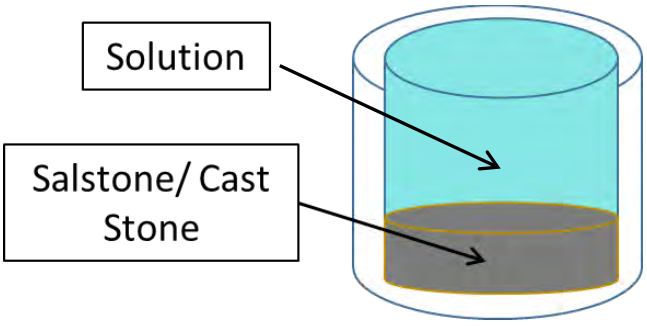

Figure 26: Experimental Setup of the Corrosion of Saltstone and Cast Stone Study

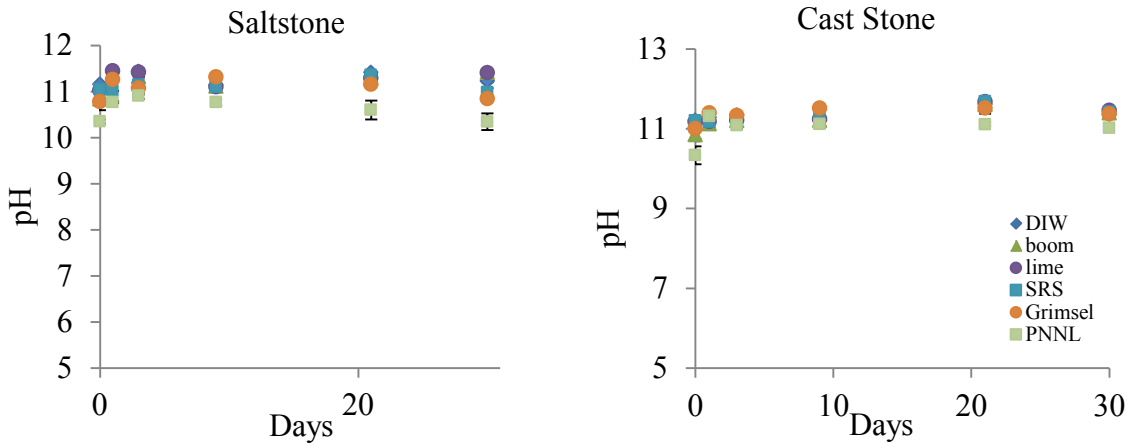

Figure 27. pH evolution during cement alterations in low ionic strength groundwaters

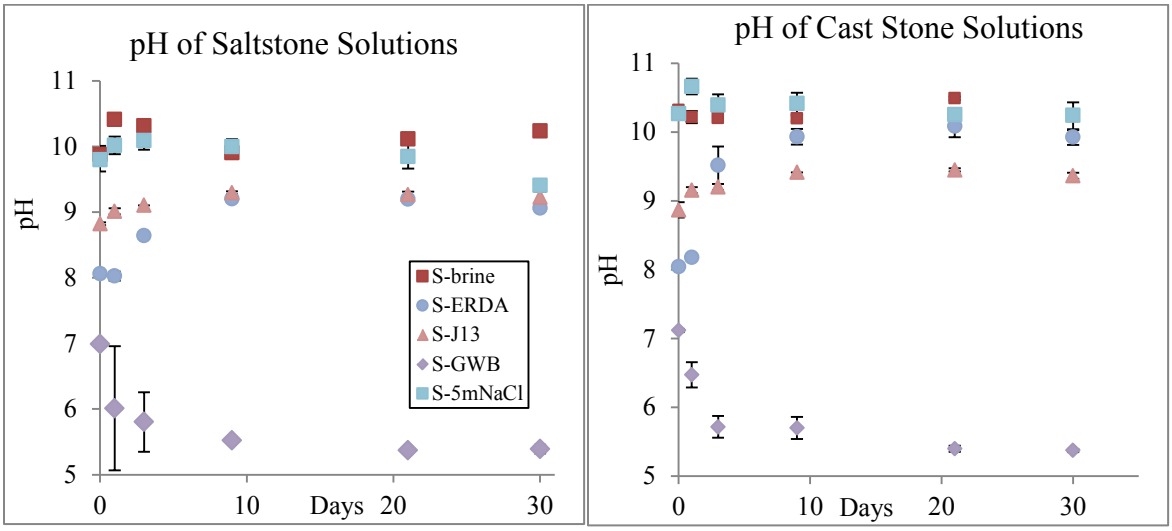

Figure 28. pH for cements in high ionic strength groundwaters.

Figure 27 demonstrates that solution pH values rapidly increase to pH 11 in groundwater of low ionic strengths. However, groundwaters of high ionic strengths show different pattern, as observer with **Figure 28**, with an equilibrium pH below 6 for GWB, a WIPP-representative brine particularly concentrated in Mg. J13 and ERDA equilibrate at ca. pH 9 and S-brine and 5 m NaCl at ca. pH 10.

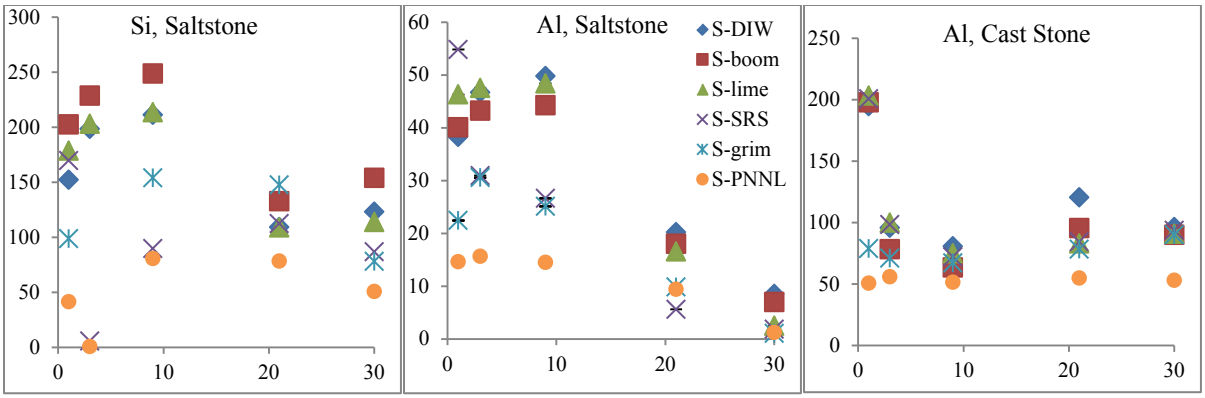

Figure 29. Elemental (Si and Al in ppm) release during alteration of Salstone and Cast Stone, in different low ionic strength groundwaters

Figure 29 indicates an elemental release smaller than precipitation during the first day(s), followed by a consumption of elements from the solution. Secondary phase(s) may be forming at that point.

Additionally, phase(s) containing Cr in the Cast Stone is(are) dissolving at an apparent constant rate throughout the experiment, as seen with **Figure 30**.

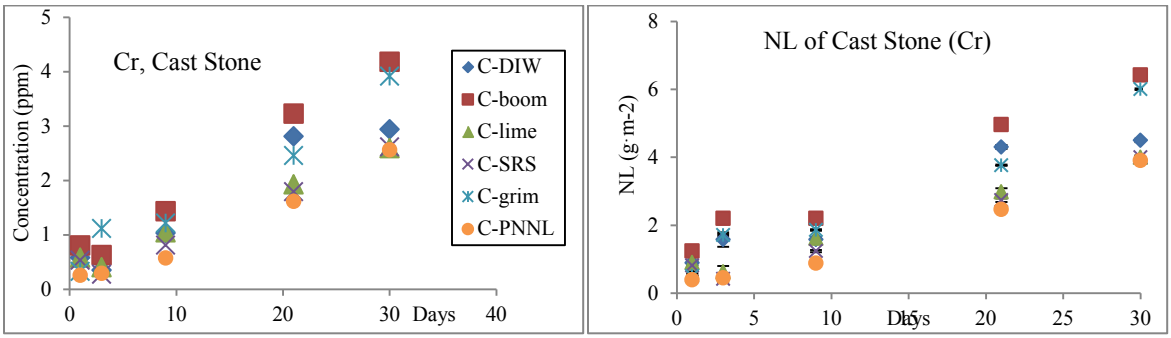

Figure 30. Cr analyses for Cast Stone

SEM analyses of various surfaces resulting from these experiments demonstrate alteration of the cements, but little can be deducted from these, due to lack of result consistency from one system to another (**Figure 31**).

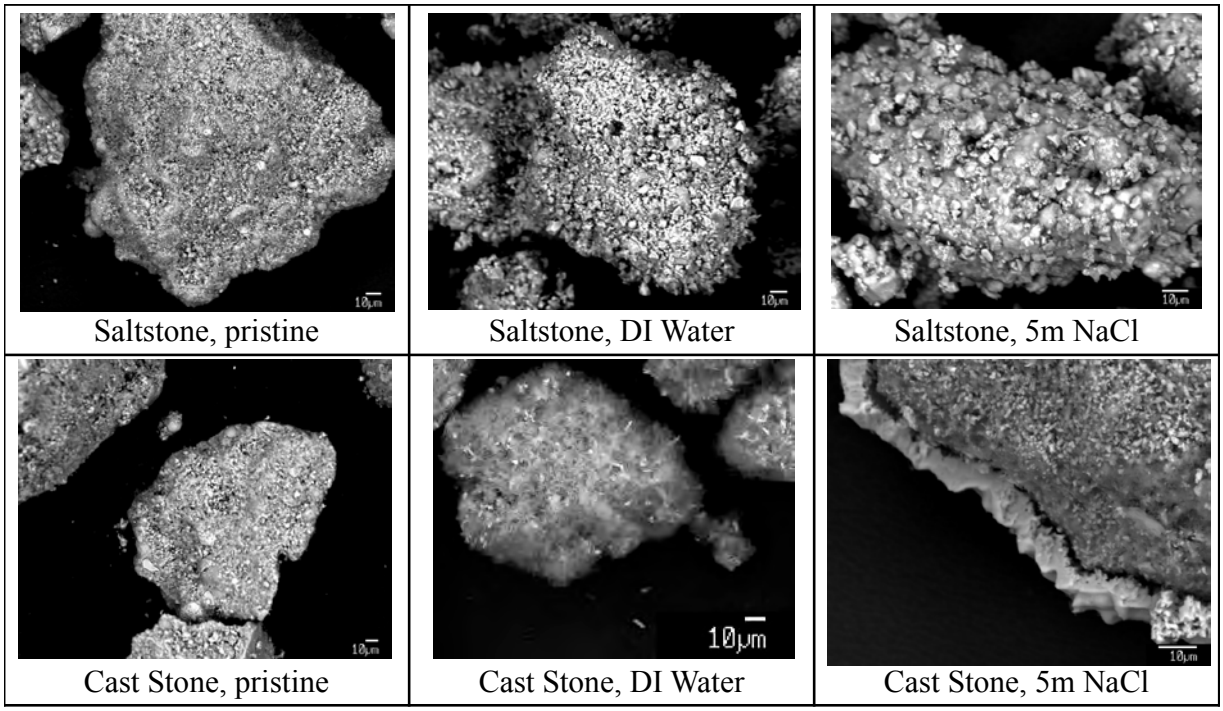

Figure 31. SEM analyses of various cementitious materials before and after alteration in groundwaters.

Bulk quantification of the samples was achieved with XRF. Samples were prepared using 2 g of wasteform sample and diluted 1) with quartz dilution (to reach 40 % of wasteform) and 2) lithium tetraborate (mass equal to twice the mass of wasteform and quartz dilution added together).Pristine sample analyses are presented with **Figure 32**. XRF analysis showed total composition percentage is around 80%. Altered cementation samples data are presented with **Figure 33**, for the main elements, and **Figure 34** for the minor elements. Data showed little to no variety in composition when various groundwaters were reacted with saltstone and cast stone, compared with the pristine samples.

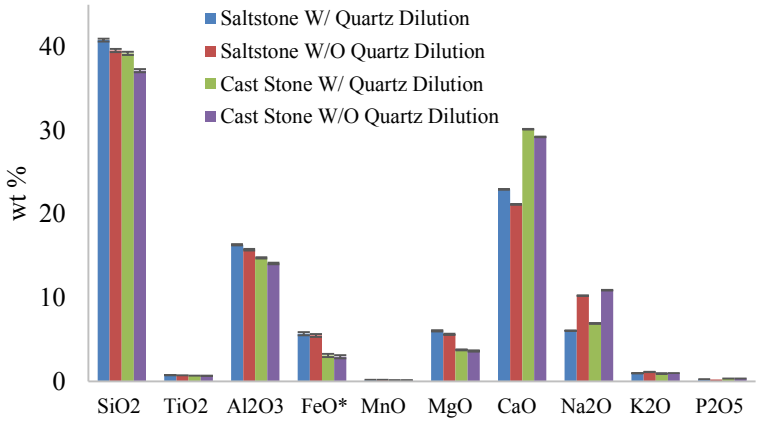

Figure 32. Initial Waste Form Bulk Simulant Characterization by XRF

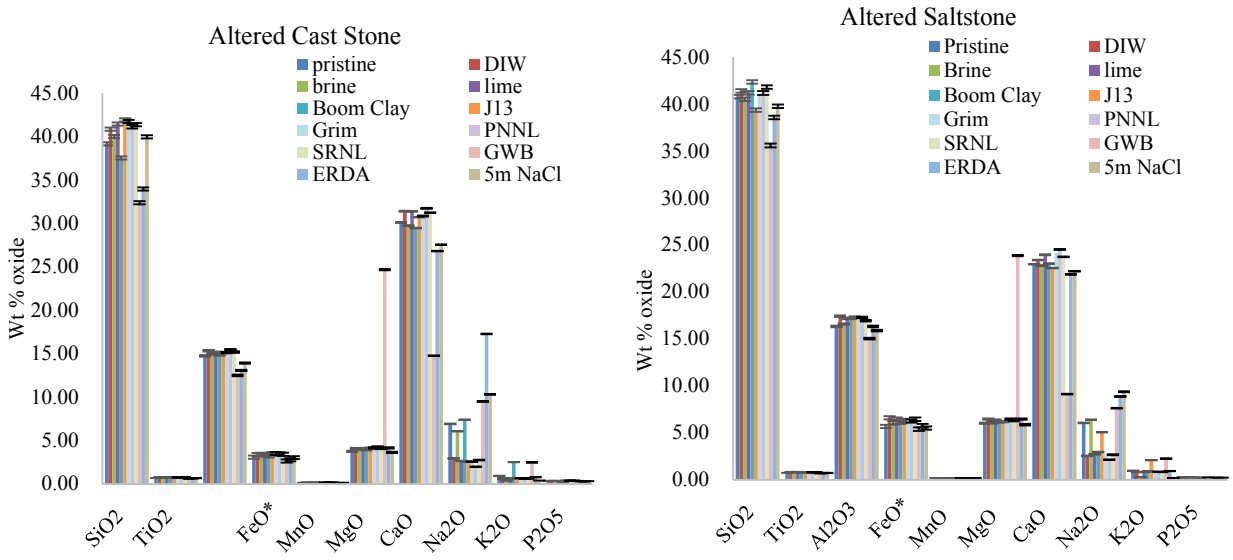

Figure 33. XRF Normalized Characterization of Main Elements

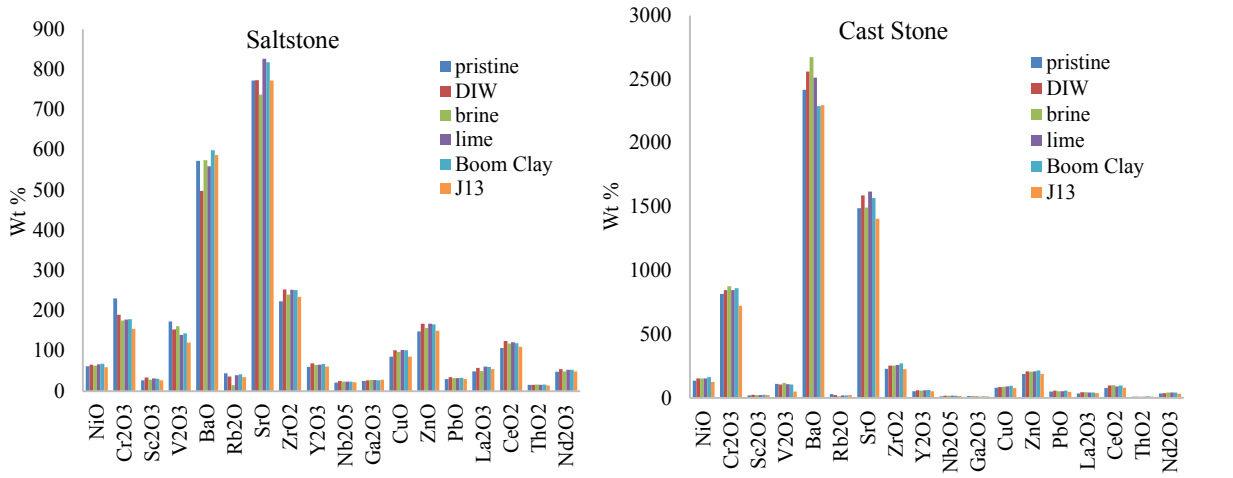

Figure 34. XRF Normalized Characterization of minor Elements

12 Corrosion of ISG in the Presence of Metals Contained in Stainless Steel

The corrosion of ISG in the presence of iron mineral and Fe^0 was extended to study the corrosion of ISG in the presence of stainless steel. Samples were prepared in a similar was in the corrosion suppressant study (section 9), using stainless steel instead of iron. We were particularly interested in the corrosion of ISG by chromium and nickel contained in stainless steel. **Figure 35** shows the experimental setup, using the smaller 0.127 mm spacer. Unfortunately, no reaction was observed within the time frame and those conditions.

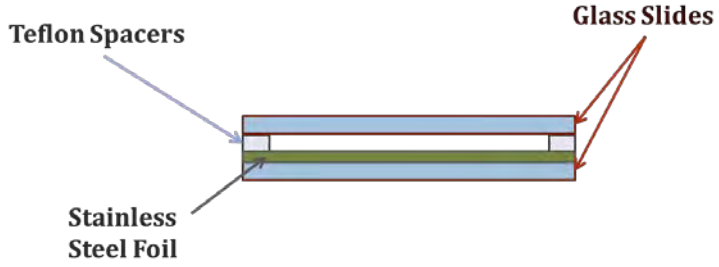

Figure 35: Setup for the Corrosion of ISG in the Presence of Metals Contained in Stainless Steel

13 Pore size analysis of the alteration layer – Positron Annihilation

Some of the ISG coupons from the corrosion suppressant study (section 9) were analyzed using Doppler broadening positron annihilation spectroscopy (PAS) to analyze nano-pores of alteration layers.

13.1 Experimental

Temperature	90°C
Glass form	2 glass coupons Eventually in contact with Fe^0 or Hematite
S/V ratio	0.4 cm^{-1} *based on geometric surface area*
Solution composition	18.2 MΩ·cm water
pH	Free, initially neutral
Duration	Static; 1, 2 or 3 months

Table 16: Summary of experimental conditions for pore size analysis experiments

Experiments were performed on ISG coupons reacted in contact with Fe, ISG coupons reacted in contact with hematite coupon, ISG coupons reacted first with hematite for 1 month then with Fe, and ISG coupons reacted first with Fe for 1 month then with hematite. These samples were analyzed with positron annihilation spectroscopy.

13.2 Preliminary results

Figure 36 shows normalized S signal measured by PAS as a function of depth. The S parameter corresponds to positron annihilation with the valence electrons which are sensitive to open volume defects. (Doppler Broadening powerpoint) An S signal of 1.00 corresponds to the vacancy of pristine ISG, and higher S signals correspond to materials that contain more vacancies than pristine ISG.

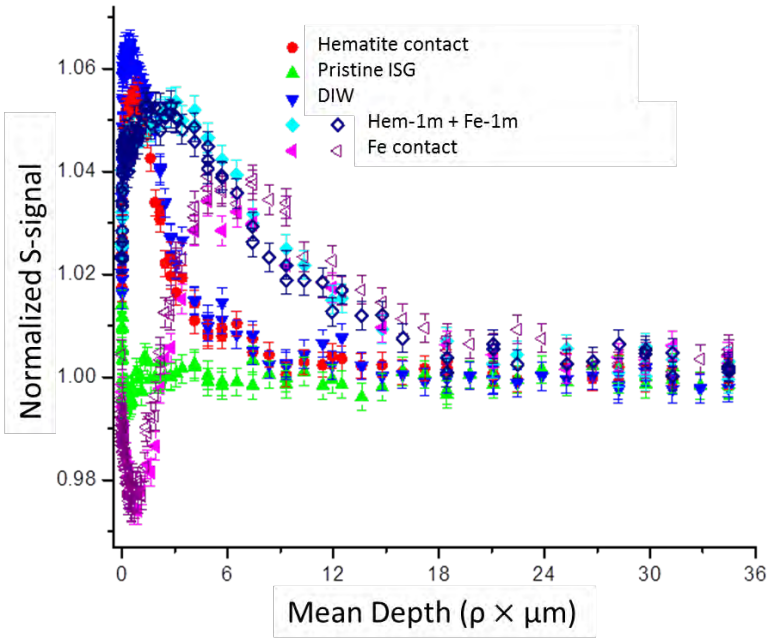

Figure 36: Normalized S-depth profile of altered and unaltered ISG as a function of depth

All the samples except ISG in contact with Fe show that the alteration layer (which corresponds to approximately 10 µm) contains more vacancies then pristine ISG whereas ISG with Fe contains less vacancies in its visible alteration layer (which corresponds to approximately 1.5 µm) than pristine ISG. However, ISG with Fe has more vacancies deeper in the sample before the vacancies return to the amount expected in the pristine glass.

Ongoing experiments are being performed in the same conditions for 2 months and 3 months. These samples will be analyzed using the same techniques and compared with the previous samples.

14 Glass alteration under irradiation

This task consists in investigating glass corrosion under gamma irradiation in presence of iron and iron corrosion products. The work is performed at the WSU Nuclear Radiation Center (WSU-NRC), using the Co-60 source facilities, in close collaboration with the WSU NRC staff.

To perform alteration experiments under irradiation, all alteration vials have been designed to avoid contamination of the samples by:

- degradation compounds from the irradiated vials: this excludes the use of any plastic in the design (including for joints);
- dissolution of gases, such as the CO_2 present in the atmosphere or nitric species generated during radiolysis in presence of N_2.

To avoid these issues, long-term alteration vials are made of inert, radiation-resistant, titanium alloy and their airtightness will be insured by a non-organic joint (silicon, graphite, metallic). Samplings are to be performed in an Argon glove box to avoid any nitrogen contamination, with double confinement to ensure a renewed high Ar purity inside the vial after each sampling. Finally, a heating system able to maintain the temperature at 90°C for several months and sized for the constrained dimensions of the Co-60 gamma irradiator at the WSU-NRC.

A sample holder accessorize with a thermocouple to maintain constant temperature and a rotator to maintain constant irradiation of the sample was designed and built to fit in the irradiator. A picture of it is shown on **Figure 37**.

Figure 37. Irradiation sample holder

SON68 glass alteration in presence of Fe powder (> 180 µm, m_{Glass}/m_{Fe} = 12.5) and under different irradiation does was investigated.

The experimental matrix followed for this experiment is presented below:

Dose rate : Temperature :	155 Gy/h 45-50°C	30 Gy/h 45-50°C	- 25°C	- 50°C
18.2 MΩ·cm water	✓	✓		
Water + Fe	✓	✓	✓	✓
Water + Glass	✓	✓	✓	✓
Water + Glass + Fe	✓	✓	✓	✓
SiO_2 solution	✓	✓	✓	✓
SiO_2 solution + Glass	✓	✓	✓	✓

Table 17. Glass alteration under irradiation experimental matrix

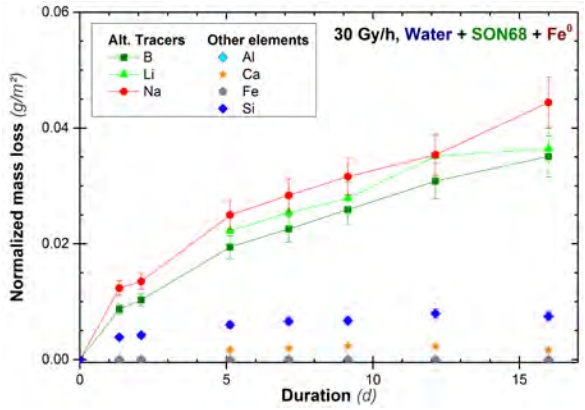

Figure 38. Normalized loss of irradiated SON68 based on different tracer, in presence of Fe^0.

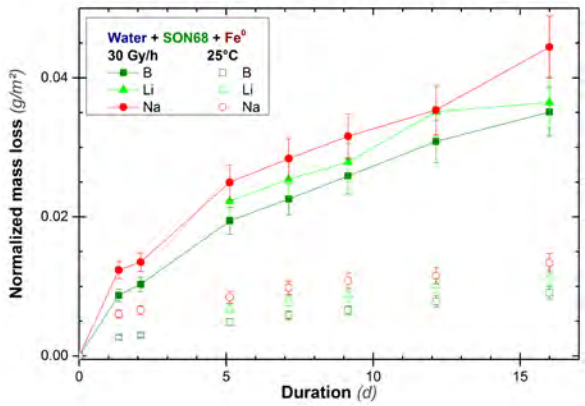

Figure 39. Normalize loss of irradiated SNO68 at 25ºC and 50ºC in presence of Fe^0.

Figure 38 shows a congruent normalized mass loss of SON68 upon 30 Gy/h irradiation among the different tracers and **Figure 39** shows a significantly lower mass loss at lower temperature.

Although solution pH remain constant at both temperature, both irradiation does, and in presence and absence of Fe (**Figure 40**), the normal mass loss is greatly affected by the irradiation at 25ºC (**Figure 41**). The effect of dose and Fe on the normal mass loss is insignificant for 15 days samples and long-term samples are currently being processed. The instantaneous SON68 alteration rates between 0 and 15 days upon an 30 Gy/h irradiation and in presence of Fe^0 are presented on **Figure 42** – we can observe again a congruent behavior of B, Li, and Na. Although

no Fe was detected in the 2 weeks samples, Fe moieties were observed in the samples (**Figure 43**).

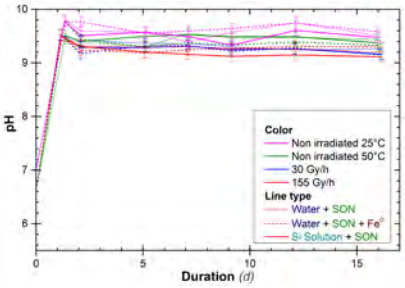

Figure 40. Solution pH of various glass alteration irradiation samples

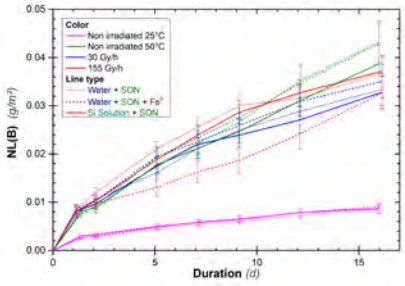

Figure 41. Normal mass loss (based on B) of various glass alteration irradiation samples

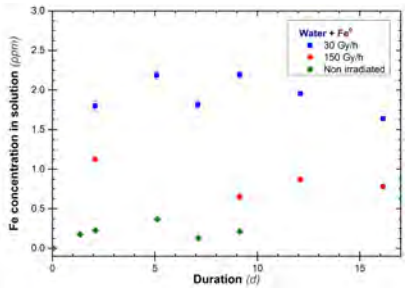

Figure 42. Instantaneous SON68 alteration rate

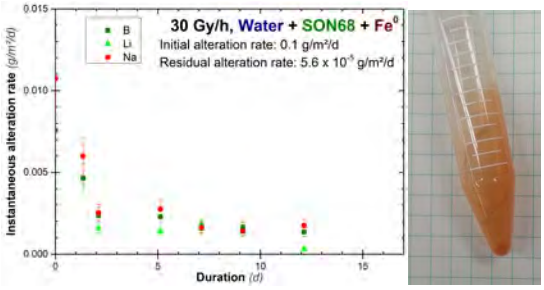

Figure 43. Fe concentration upon sample irradiation and visual sample observation

These experiments will be continued over the next few months.

15 Communications and Awards

(Visiting scientist[&], Research Assistant/Post-Doctoral Fellows[@], Graduate Student[#], Undergraduate Student [$])

15.1 Communications:

15.1.1 Presentations

Nuclear waste glass alteration under gamma irradiation in presence of near field materials Parruzot, B.@; Waters, S.M.; Wall, D.E.; Neeway, J.J.; Ryan, J.V.; Gin, S.; Wall, N.A. Methods and Applications of Radioanalytical Chemistry, Kailua-Kona, HI 04/12-17/2015

Corrosion of salstone and castone by nuclear waste repository groundwaters. Reiser, J.T.#; Riggan, B.K.$; Musa C.M.$; Parruzot, B. @; Neeway, J.J.; Ryan, J.V.; Qafoku, N.; Wall, N.A. Methods and Applications of Radioanalytical Chemistry, Kailua-Kona, HI 04/12-17/2015

Determination of mineral surface area by methylene blue sorption: comparison with BET and geometric surface areas. Parruzot, B.@; Reiser, J.T.#; Riggan, B.K.$; Wall, N.A. Methods and Applications of Radioanalytical Chemistry, Kailua-Kona, HI 04/12-17/2015

Effect of iron-bearing environment on the alteration of SON68 and ISG glasses. Lemesle T.@, Cecilia Eiroa Lledo$, Neeway J.J., Ryan J.V., McCloy J.S., Wall N. Methods and Applications of Radioanalytical Chemistry, Kailua-Kona, HI 04/12-17/2015

Effect of solution composition on the alteration of the SON68 and ISG glasses. Lemesle T. @, Cecilia Eiroa Lledo$, Neeway J.J., Ryan J.V., Qafoku N., McCloy J.S., Wall N. Methods and Applications of Radioanalytical Chemistry, Kailua-Kona, HI 04/12-17/2015

Effect of the surface/volume ratio on the alteration of SON68 and ISG glasses. Lemesle T. @, Cecilia Eiroa Lledo$, Neeway J.J., Ryan J.V., Qafoku N., McCloy J.S., Wall N. Methods and Applications of Radioanalytical Chemistry, Kailua-Kona, HI 04/12-17/2015

Incorporation of iodine in phosphate-based glass. Lemesle T., Mear F.O., Campayo L., Pinet O., Montagne L., Wall N.A. 248th ACS Fall meeting, San Francisco CA, 08/10-14/2014

A Sampling Method for Semi-Quantitative and Quantitative Electron Microprobe Analysis of Glass Surfaces. Jamie L. Weaver#, Joelle Reiser#, Owen K. Neill, John S. McCloy, Nathalie A. Wall. Glass & Optical Materials Division and Deutsche Glastechnische Gesellschaft Joint Annual Meeting 2015, Miami, FL, 05/17-21/2015

Glass corrosion in the presence of iron-bearing materials and potential corrosion suppressors. Joelle Reiser#, Lindsey Neill#, Benjamin Parruzot@, Jamie Weaver#, Christopher Musa$, James Neeway, Joseph Ryan, Nikolla Qafoku, Stéphane Gin, Nathalie A. Wall. Glass & Optical Materials Division and Deutsche Glastechnische Gesellschaft Joint Annual Meeting 2015, Miami, FL, 05/17-21/2015

A Cross-Sectional Sampling Method for Quantitative and Qualitative Electron Microprobe Analysis of Simulated Nuclear Waste Glasses. Jamie L. Weaver, Joelle Reiser, Owen K. Neill, John McCloy, Nathalie A. Wall. 2014 MRS Fall meeting, Boston, MA, 11/30-12/05/2014

Glass corrosion in the presence of iron-bearing materials and potential corrosion suppressors. Joelle Reiser, Lindsey Neill, Jamie Weaver, Christopher Musa, James Neeway, Joseph Ryan, Nikolla Qafoku, Stéphane Gin, Nathalie A. Wall.2014 MRS Fall meeting, Boston, MA, 11/30-12/05/2014

Overview of Gaps in High-Level Nuclear Waste Form/Near-Field Material Interactions. Jim Neeway, Nik Qafoku, Joe Ryan, Joelle Reiser, Lindsey Neill, Jamie Weaver, Nathalie Wall. 51st Annual Meeting of The Clay and Minerals Society, Texas A & M, College Station, TX, 05/17-21/2014

Making Nuclear Waste Glass Last: How studying ancient glasses can help predict the long-term durability of nuclear waste glasses. Jamie Weaver#, David Peeler, Rolf Sjöblom, John McCloy, Nathalie A. Wall, Michael Schweiger, and Albert Kruger. Waste Management 2016, Phoenix, AZ 03/06-10/2016

Update on the Synthesis and Characterization of Alkali Technetium Oxides as Model Compounds for Tc-99 Incorporation in Glass. Jamie Weaver#, Nathalie A. Wall, Chuck Soderquist, John McCloy. Material Science and Technology 2015, Columbus, OH, 10/04-08/2015

Alkali technetium oxides as model compounds for Tc-99 incorporation in glass. Jamie Weaver#, Nathalie A. Wall, Chuck Soderquist, John McCloy. ACS 250th National Meeting, Boston, MA, 08/15-20/2015

Colored and Colorless Roman Glass: Using Ancient Artifacts to Solve Modern Challenges in Glass Corrosion Science. Jamie Weaver#. Presentations at the British Museum, London. UK

The Use of Pure Tc-99 Compounds as Standards for Tc in Nuclear Waste Glass. Jamie Weaver#. Presentations at the British Museum, London. UK

Alkali Technetium Oxides as Model Compounds for 99Tc Incorporation in Glass. Jamie Weaver#, John McCloy, Chuck Soderquist. Glass & Optical Materials Division and Deutsche Glastechnische Gesellschaft Joint Annual Meeting 2015, Miami, FL, 05/17-21/2015.

A Sampling Method for Semi-Quantitative and Quantitative Electron Microprobe Analysis of Glass Surfaces. Jamie L. Weaver#, Joelle Reiser#, Owen K. Neill, John S. McCloy, Nathalie A. Wall. Glass & Optical Materials Division and Deutsche Glastechnische Gesellschaft Joint Annual Meeting 2015, Miami, FL, 05/17-21/2015

Glass corrosion in the presence of iron-bearing materials and potential corrosion suppressors. Joelle Reiser#, Lindsey Neill#, Benjamin Parruzot@, Jamie Weaver#, Christopher Musa$, James Neeway, Joseph Ryan, Nikolla Qafoku, Stéphane Gin, Nathalie A. Wall. Glass & Optical Materials Division and Deutsche Glastechnische Gesellschaft Joint Annual Meeting 2015, Miami, FL, 05/17-21/2015

Wet Chemical and UV-Vis Spectrometric Iron Speciation in Quenched Low and Intermediate Level Nuclear Waste Glasses. Jamie L. Weaver, Nathalie A. Wall, John McCloy. 2014 MRS Fall meeting, Boston, MA, 11/30-12/05/2014.

A Cross-Sectional Sampling Method for Quantitative and Qualitative Electron Microprobe Analysis of Simulated Nuclear Waste Glasses. Jamie L. Weaver, Joelle Reiser, Owen K.

Neill, John McCloy, Nathalie A. Wall. 2014 MRS Fall meeting, Boston, MA, 11/30-12/05/2014.

Overview of Gaps in High-Level Nuclear Waste Form/Near-Field Material Interactions. Jim Neeway, Nik Qafoku, Joe Ryan, Joelle Reiser, Lindsey Neill, Jamie Weaver, Nathalie Wall. 51st Annual Meeting of The Clay and Minerals Society, Texas A & M, College Station, TX, 05/17-21/2014

Effects of Near Field Materials on Glass Corrosion. Neill L# and Wall N.A. Sixth International Glass Corrosion Workshop. Coronado, CA 05/31-06/01/2013.

Aspects of technetium chemistry for nuclear waste management. N.A. Wall. ACS 247th National Meeting, Dallas, TX, 03/16-20/2014.

15.1.2 Publications

Wet Chemical and UV-Vis Spectrometric Iron Speciation in Low and Intermediate Level Nuclear Waste Glasses. Jamie L. Weaver#, Nathalie A. Wall, John S. McCloy. MRS Proceedings - 1744(Scientific Basis for Nuclear Waste Management XXXVIII), 1-8 (2015) DOI:10.1557/opl.2015.481

A Sampling Method for Semi-Quantitative and Quantitative Electron Microprobe Analysis of Glass Surfaces. Jamie L. Weaver#, Joelle Reiser#, Owen K. Neill, John S. McCloy, Nathalie A. Wall. MRS Proceedings 1744(Scientific Basis for Nuclear Waste Management XXXVIII), 1-6 (2015)
DOI:10.1557/opl.2015.496
N. Wall is a corresponding author; she supervised the work performed by the graduate and edited the paper drafts.

Glass corrosion in the presence of iron-bearing materials and potential corrosion suppressors. Joelle Reiser#, Lindsey Neill#, Benjamin Parruzot@, Jamie Weaver#, Christopher Musa$, James Neeway, Joseph Ryan, Nikolla Qafoku, Stéphane Gin, Nathalie A. Wall. MRS Proceedings 1744(Scientific Basis for Nuclear Waste Management XXXVIII), 1-6. (2015) DOI:10.1557/o*pl.2015.503*

Influence of the presence of salt in solution on the alteration of ISG and SON 68 glasses. Thomas Lemesle, James J. Neeway, Joseph V. Ryan, Nikolla P. Qafoku, John McCloy, Nathalie A. Wall. *In preparation*.

Alteration of ISG and SON 68 glasses in presence of hematite. Thomas Lemesle, James J. Neeway, Joseph V. Ryan, Nikolla P. Qafoku, John McCloy, Nathalie A. Wall. *In preparation*

Additional publications will be submitted in the next 2 years, presenting data related to this project.

15.2 Awards:

Lindsey Neill: 2014 Chateaubriand Fellowship – Science, Technology, Engineering & Mathematics (STEM). Grant offered by the Office for Science and Technology (OST) of the Embassy of France in the United States. Recipient receives monthly allowance, support for travel to and from France, and support for health insurance abroad. This award allows Ms. Neill to work for 9 months with Dr. Gin at the CEA (France), where she will conduct

experimental work for understanding silicon behavior between the glass network and leaching solution by using a ^{29}Si tracer to understand the structure of the amorphous layer on altered glass, in presence and absence of an iron source.

Lindsey Neill: 2014 Jim and Lee Ella Ruck Graduate Fellowship in Chemistry. This award recognizes academic achievements and the promise they show for continued professional development.

Jamie Weaver: 2015 Golding Family Women in Science Fellowship

15.3 Miscellaneous

Lindsey Neill: Internship at the French Atomic Energy Agency (Commissariat à l'Energie Atomique) – 9 months (09/2014-05/2015) –, working with Dr. Gin on aspects of glass corrosion, for application to nuclear waste management. Funded by the aforementionned 2014 Chateaubriand Fellowhip, N.A. Wall's NEUP grant, and CEA.

Jamie Weaver: 2015 PhD Intern position within the Energy and Environment Directorate of the Pacific Northwest National Laboratory (PNNL).

N.A. Wall was awarded Tenure and promotion to Associate Professor of Chemistry in 2015.

16 References

1. Gin, S.; Abdelouas, A.; Criscenti, L. J.; Ebert, W. L.; Ferrand, K.; Geisler, T.; Harrison, M. T.; Inagaki, Y.; Mitsui, S.; Mueller, K. T.; Marra, J. C.; Pantano, C. G.; Pierce, E. M.; Ryan, J. V.; Schofield, J. M.; Steefel, C. I.; Vienna, J. D., An international initiative on long-term behavior of high-level nuclear waste glass. *Materials Today* **2013,** *16* (6), 243-248.
2. Ong, S. W.; Zhao, X. L.; Eisenthal, K. B., POLARIZATION OF WATER-MOLECULES AT A CHARGED INTERFACE - 2ND HARMONIC STUDIES OF THE SILICA WATER INTERFACE. *Chemical Physics Letters* **1992,** *191* (3-4), 327-335.
3. Inagaki, Y.; Kikunaga, T.; Idemitsu, K.; Arima, T., Initial Dissolution Rate of the International Simple Glass as a Function of pH and Temperature Measured Using Microchannel Flow-Through Test Method. *International Journal of Applied Glass Science* **2013,** *4* (4), 317-327.
4. Neeway, J. J.; Abdelouas, A.; Ribet, S.; El Mendili, Y.; Schumacher, S.; Grambow, B., Effect of Callovo-Oxfordian clay rock on the dissolution rate of the SON68 simulated nuclear waste glass. *Journal of Nuclear Materials* **2015,** *459*, 291-300.
5. Ribet, I.; Gin, S.; Godon, N.; Jollivet, P.; Minet, Y.; Grambow, B.; Abdelouas, A.; Ferrand, K.; Lemmens, K.; Aertsens, M.; Pirlet, V.; Jacques, D.; Crovisier, J. L.; Clément, A.; Fritz, B.; Munier, I.; Del Nero, M.; Ozgümüs, A.; Curti, E.; Luckscheiter; Schwyn, B. *Long-term behaviour of glass: Improving the glass source term and substantiating the basic hypotheses (GLASTAB)*; European Atomic Energy Community: 2007.
6. Chave, T.; Frugier, P.; Gin, S.; Ayral, A., Glass-water interphase reactivity with calcium rich solutions. *Geochimica Et Cosmochimica Acta* **2011,** *75* (15), 4125-4139.
7. Majerus, O.; Gerardin, T.; Manolescu, G.; Barboux, P.; Caurant, D., Effect of aqueous Mg2+ and Ca2+ cations on the dissolution kinetics and alteration layer of sodium borosilicate glasses at neutral pH buffered with Tris/HCI. *Physics and Chemistry of Glasses-European Journal of Glass Science and Technology Part B* **2014,** *55* (6), 261-273.
8. Thien, B. M. J.; Godon, N.; Ballestero, A.; Gin, S.; Ayral, A., The dual effect of Mg on the long-term alteration rate of AVM nuclear waste glasses. *Journal of Nuclear Materials* **2012,** *427* (1-3), 297-310.
9. Gin, S.; Beaudoux, X.; Angeli, F.; Jegou, C.; Godon, N., Effect of composition on the short-term and long-term dissolution rates of ten borosilicate glasses of increasing complexity from 3 to 30 oxides. *Journal of Non-Crystalline Solids* **2012,** *358* (18-19), 2559-2570.
10. Reiser, J.; Neill, L.; Weaver, J.; Parruzot, B.; Musa, C.; Neeway, J.; Ryan, J.; Qafoku, N.; Gin, S.; Wall, N. A., Glass corrosion in the presence of iron-bearing materials and potential corrosion suppressors. *MRS Online Proc. Libr.* **2015,** *1744* (Scientific Basis for Nuclear Waste Management XXXVIII), 1-6.
11. McGrail, B. P.; Lindenmeier, C. W.; Martin, P. F. C.; Gee, G. W., The pressurized unsaturated flow (PUF) test: A new method for engineered-barrier materials evaluation. *Ceram. Trans.* **1996,** *72* (Environmental Issues and Waste Management Technologies in the Ceramic and Nuclear Industries II), 317-329.

12. McGrail, B. P.; Lindenmeier, C. W.; Martin, P. F., Characterization of pore structure and hydraulic property alteration in pressurized unsaturated flow tests. *Mater. Res. Soc. Symp. Proc.* **1999,** *556* (Scientific Basis for Nuclear Waste Management XXII), 421-428.
13. McGrail, B. P.; Martin, P. F.; Schaef, H. T.; Lindenmeier, C. W.; Owen, A. T., Glass/ceramic interactions in the can-in-canister configuration for disposal of excess weapons plutonium. *Mater. Res. Soc. Symp. Proc.* **2000,** *608* (Scientific Basis for Nuclear Waste Management XXIII), 345-352.
14. Pierce, E. M.; McGrail, B. P.; Valenta, M. M.; Strachan, D. M., The accelerated weathering of a radioactive low-activity waste glass under hydraulically unsaturated conditions: experimental results from a pressurized unsaturated flow test. *Nucl. Technol.* **2006,** *155* (2), 149-165.
15. Wierenga, P. J.; Young, M. H.; Gee, G. W.; Hills, R. G.; Kincaid, C. T.; Nicholson, T. J.; Cady, R. E. *Soil Characterization Methods for Unsaturated Low-Level Waste Sites.*; Pacific Northwest Laboratory: Richland, WA, USA, 1993.
16. Michelin, A.; Burger, E.; Leroy, E.; Foy, E.; Neff, D.; Benzerara, K.; Dillmann, P.; Gin, S., Effect of iron metal and siderite on the durability of simulated archeological glassy material. *Corrosion Science* **2013,** *76*, 403-414.
17. Nielsen, C. H.; Sigurdsson, H., Quantitative methods for electron microprobe analysis of sodium in natural and synthetic glasses. *Am. Mineral.* **1981,** *66* (5-6), 547-52.
18. Grambow, B., Nuclear waste glasses - How durable? *Elements* **2006,** *2* (6), 357-364.
19. Hunter, R. T.; Edge, M.; Kalivretenos, A.; Brewer, K. M.; Brock, N. A.; Hawkes, A. E.; Fanning, J. C., DETERMINATION OF THE FE2+/FE3+ RATIO IN NUCLEAR WASTE GLASSES. *Journal of the American Ceramic Society* **1989,** *72* (6), 943-947.
20. Fanning, J. C.; Hunter, R. T., NUCLEAR WASTE, GLASS, AND THE FE-2+/FE-3+ RATIO. *Journal of Chemical Education* **1988,** *65* (10), 888-889.
21. Muller, I. S.; Viragh, C.; Gan, H.; Matlack, K. S.; Pegg, I. L., Iron Moessbauer redox and relation to technetium retention during vitrification. *Hyperfine Interact.* **2009,** *191* (1-3), 17-24.
22. Arletti, R.; Quartieri, S.; Freestone, I. C., A XANES study of chromophores in archaeological glass. *Appl. Phys. A: Mater. Sci. Process.* **2013,** *111* (1), 99-108.
23. Baert, K.; Meulebroeck, W.; Wouters, H.; Cosyns, P.; Nys, K.; Thienpont, H.; Terryn, H., Using Raman spectroscopy as a tool for the detection of iron in glass. *J. Raman Spectrosc.* **2011,** *42* (9), 1789-1795.
24. Jones, D. R. I. V.; Jansheski, W. C.; Goldman, D. S., Spectrophotometric determination of reduced and total iron in glass with 1,10-phenanthroline. *Anal. Chem.* **1981,** *53* (6), 923-4.
25. Klement, R.; Kraxner, J.; Liska, M., Spectroscopic analysis of iron doped glasses with composition close to the E-glass: a preliminary study. *Ceram.-Silik.* **2009,** *53* (3), 180-183.
26. Kido, L.; Mueller, M.; Ruessel, C., High temperature vis-NIR transmission spectroscopy of iron-doped glasses. *Phys. Chem. Glasses: Eur. J. Glass Sci. Technol., Part B* **2010,** *51* (4), 208-212.

27. Li, H.; Vienna, J. D.; Hrma, P.; Smith, D. E.; Schweiger, M. J., Nepheline precipitation in high-level waste glasses: compositional effects and impact on the waste form acceptability. *Mater. Res. Soc. Symp. Proc.* **1997,** *465* (Scientific Basis for Nuclear Waste Management XX), 261-268.
28. Stucki, J. W.; Anderson, W. L., The quantitative assay of minerals for iron(2+) and iron(3+) ions using 1,10-phenanthroline: I. Sources of variability. *Soil Sci. Soc. Am. J.* **1981,** *45* (3), 633-7.
29. Cochain, B.; Neuville, D. R.; Henderson, G. S.; McCammon, C. A.; Pinet, O.; Richet, P., Effects of the iron content and redox state on the structure of sodium borosilicate glasses: a Raman, Mossbauer and boron K-edge XANES spectroscopy study. *J. Am. Ceram. Soc.* **2012,** *95* (3), 962-971.
30. Kukkadapu, R. K.; Li, H.; Smith, G. L.; Crum, J. D.; Jeoung, J.-S.; Howard Poisl, W.; Weinberg, M. C., Mossbauer and optical spectroscopic study of temperature and redox effects on iron local environments in a Fe-doped (0.5 mol% Fe2O3) 18Na2O-72SiO2 glass. *J. Non-Cryst. Solids* **2003,** *317* (3), 301-318.
31. Melcher, M.; Wiesinger, R.; Schreiner, M., Degradation of Glass Artifacts: Application of Modern Surface Analytical Techniques. *Accounts of Chemical Research* **2010,** *43* (6), 916-926.
32. Bingham, P. A.; Jackson, C. M., Roman blue-green bottle glass: chemical-optical analysis and high temperature viscosity modelling. *Journal of Archaeological Science* **2008,** *35* (2), 302-309.
33. Bellendorf, P.; Gerlach, G.; Mottner, P.; López, E., *Glass & Ceramic Conservation 2010,*. Inter. Coun. Muse. Symp. Proc. Corning, : New York, 2010.
34. Boudreault, J.-P.; Dube, J.-S.; Sona, M.; Hardy, E., Analysis of procedures for sampling contaminated soil using Gy's Sampling Theory and Practice. *Sci. Total Environ.* **2012,** *425*, 199-207.
35. Geisler, T.; Janssen, A.; Scheiter, D.; Stephan, T.; Berndt, J.; Putnis, A., Aqueous corrosion of borosilicate glass under acidic conditions: A new corrosion mechanism. *Journal of Non-Crystalline Solids* **2010,** *356* (28-30), 1458-1465.
36. Newbury, D. E., Misidentification of major constituents by automatic qualitative energy dispersive X-ray microanalysis: A problem that threatens the credibility of the analytical community. *Microscopy and Microanalysis* **2005,** *11* (6), 545-561.
37. Standards, A., ASTM C1285. Annual Book of ASTM Standards, Vol. 12.01: Standard Test Methods for Determining Chemical Durability of Nuclear, Hazardous, and Mixed Waste Glasses and Multiphase Glass Ceramics: The Product Consistency Test (PCT).
38. Bastin, G. F.; Dijkstra, J. M.; Heijligers, H. J. M., PROZA96: an improved matrix correction program for electron probe microanalysis, based on a double gaussian phi(rho z) approach. *X-Ray Spectrometry* **1998,** *27* (1), 3-10.
39. Chaussidon, M.; Robert, F.; Mangin, D.; Hanon, P.; Rose, E. F., Analytical procedures for the measurement of boron isotope compositions by ion microprobe in meteorites and mantle rocks. *Geostandards Newsletter-the Journal of Geostandards and Geoanalysis* **1997,** *21* (1), 7-17.